



3 4456 0510973 5

ORNL-5777

ornl

**OAK
RIDGE
NATIONAL
LABORATORY**



Calculational Procedures for the Analysis of Integral Experiments for Fusion Reactor Design

R. T. Santoro
J. M. Barnes
R. G. Alsmiller, Jr.
E. M. Obler

OAK RIDGE NATIONAL LABORATORY
CENTRAL RESEARCH LIBRARY
CIRCULATION SECTION
4500N ROOM 175
LIBRARY LOAN COPY
DO NOT TRANSFER TO ANOTHER PERSON
If you wish someone else to see this
report, send its name with report and
the library will arrange a loan.
OCT 1968

OPERATED BY
UNION CARBIDE CORPORATION
FOR THE UNITED STATES
DEPARTMENT OF ENERGY

Printed in the United States of America. Available from
National Technical Information Service
U. S. Department of Commerce
5285 Port Royal Road, Springfield, Virginia 22161
NTIS price codes: MF01/PCOPY/AGA/Microfilm/AG1

This report was prepared as an account of work sponsored by an agency of the United States Government. Neither the United States Government nor any agency thereof, nor any of their employees, makes any warranty, express or implied, or assumes any legal liability or responsibility for the accuracy, completeness, or usefulness of any information, apparatus, product, or process disclosed, or represents that its use would not infringe privately owned rights. Reference herein to any specific commercial product, process, or service by trade name, trademark, manufacturer, or otherwise, does not necessarily constitute or imply its endorsement, recommendation, or favoring by the United States Government or any agency thereof. The views and opinions of authors expressed herein do not necessarily state or reflect those of the United States Government or any agency thereof.

ORNL-5777
Dist. Category UC-20d

Contract No. W-7405-eng-26
Engineering Physics Division

CALCULATIONAL PROCEDURES FOR THE ANALYSIS OF INTEGRAL
EXPERIMENTS FOR FUSION REACTOR DESIGN

R. T. Santoro
J. M. Barnes*
R. G. Alsmiller, Jr.
E. M. Oblow

Date Published - July 1981

*Computer Sciences Division

This Work Sponsored by
Office of Fusion Energy
U. S. Department of Energy

OAK RIDGE NATIONAL LABORATORY
Oak Ridge, Tennessee 37830
operated by
UNION CARBIDE CORPORATION
for the
DEPARTMENT OF ENERGY



3 4456 0510973 5

TABLE OF CONTENTS

<u>Section</u>	<u>Page</u>
ABSTRACT	v
I. INTRODUCTION	1
II. DETAILS OF THE EXPERIMENTAL CONFIGURATION AND ANALYSIS	2
A. Experimental Facility Shield Design Calculations . . .	6
B. Optimization of the Computational Model	17
III. ENERGY ANGLE RELATIONS FOR D-T NEUTRONS	24
IV. NUCLEAR DATA PROCESSING	30
V. RADIATION TRANSPORT CALCULATIONS	36

ABSTRACT

The calculational models, nuclear data, and radiation transport codes that are used in the analysis of integral measurements of the transport of ~ 14 MeV neutrons through laminated slabs of materials typical of those found in fusion reactor shields are described. The two-dimensional discrete ordinates calculations to optimize the experimental configuration for reducing the neutron and gamma ray background levels and for obtaining an equivalent, reduced geometry of the calculational model to reduce computer core storage and running times are also presented. The equations and data to determine the energy-angle relations of neutrons produced in the reactions of 250 keV deuterons in a titanium-tritide target are given. The procedures used to collapse the ^{171}In - ^{36}Gd VITAMIN C cross section data library to a ^{53}In - ^{21}Gd broad group library are described. Finally, a description of the computer code network used to obtain neutron and gamma ray energy spectra for comparison with measured data is included. The network incorporates several two-dimensional discrete ordinates codes to treat first collisions (GRTUNCL), multiple collisions (DOT), and last collisions (FALSTF) of the neutrons and gamma rays in the transport sequence from the neutron source to the detector.

I. INTRODUCTION

A series of integral experiments are being carried out at the Oak Ridge National Laboratory to obtain experimental data to verify the nuclear data and radiation transport methods that are being used in nuclear shield design calculations for fusion reactors. These experiments are supported by an analytic program that provides this verification by making extensive comparisons between the measured results and those obtained from calculation.

The experiments consist of a sequence of carefully designed integral measurements that proceed from the transport of ~ 14 MeV DT neutrons through laminated slabs of materials typical of those found in fusion reactor blankets and shields to the measurements of neutrons streaming through penetrations in these assemblies. The analysis program supports the experiments with both pre- and postexperimental analyses. Preexperiment analysis provides the experimentalists with guidance in material selection, geometric configurations, systems dimensions, and other related quantities to design the experiment. In addition, sensitivity analyses are used to establish the similarity between what is to be measured and the design performance to be verified.^{1,2} When the experimental data become available, postexperiment analyses are performed to determine the capability and adequacy of the nuclear data and radiation transport methods for reproducing the measured results.³

This paper describes the calculational models, nuclear data, and radiation transport codes that were used in a two-dimensional analysis of the transport of ~ 14 MeV neutrons through laminated slabs of materials for fusion reactor shields. The purpose of the analysis was to calculate

neutron and gamma ray energy spectra as a function of detector location behind slabs of varying thickness and composition. The slabs consisted of stainless steel type 304 (SS-304), borated polyethylene (BP), and Hevimet (a tungsten alloy). The experimental configuration, the two-dimensional calculational model used to represent the experiment, and the results of analyses to establish the adequacy of experimental configuration for carrying out the measurement are summarized in Section II. The derivation of the angle-energy dependence of the D-T neutron source for inclusion in the radiation transport codes is given in Section III. The nuclear data and methods to process them are described in Section IV and the two-dimensional radiation transport code network that was developed for analysis of the attenuation experiments is summarized in Section V.

II. DETAILS OF THE EXPERIMENTAL CONFIGURATION AND ANALYSIS

The experimental facility used in carrying out the integral measurements of the transport of ~ 14 MeV neutrons in slabs of materials typical of those found in fusion reactor blankets and shields is shown in an artist's rendition in Fig. 1. A detailed description of the experimental components, neutron and gamma ray detection methods, and the data collection, storage, and processing is given in Ref. 4, so only a brief description is given here for clarifying the analytic procedures and calculational models that were adopted in the analysis.

The main components of the facility include an electrostatic generator for accelerating deuterons, a tritium target source can assembly, a concrete slab support shield, and the radiation detector system. Deuterons are accelerated to an energy of 250 keV, migrate through a drift tube, and interact in the tritium target to produce ~ 14 MeV neutrons

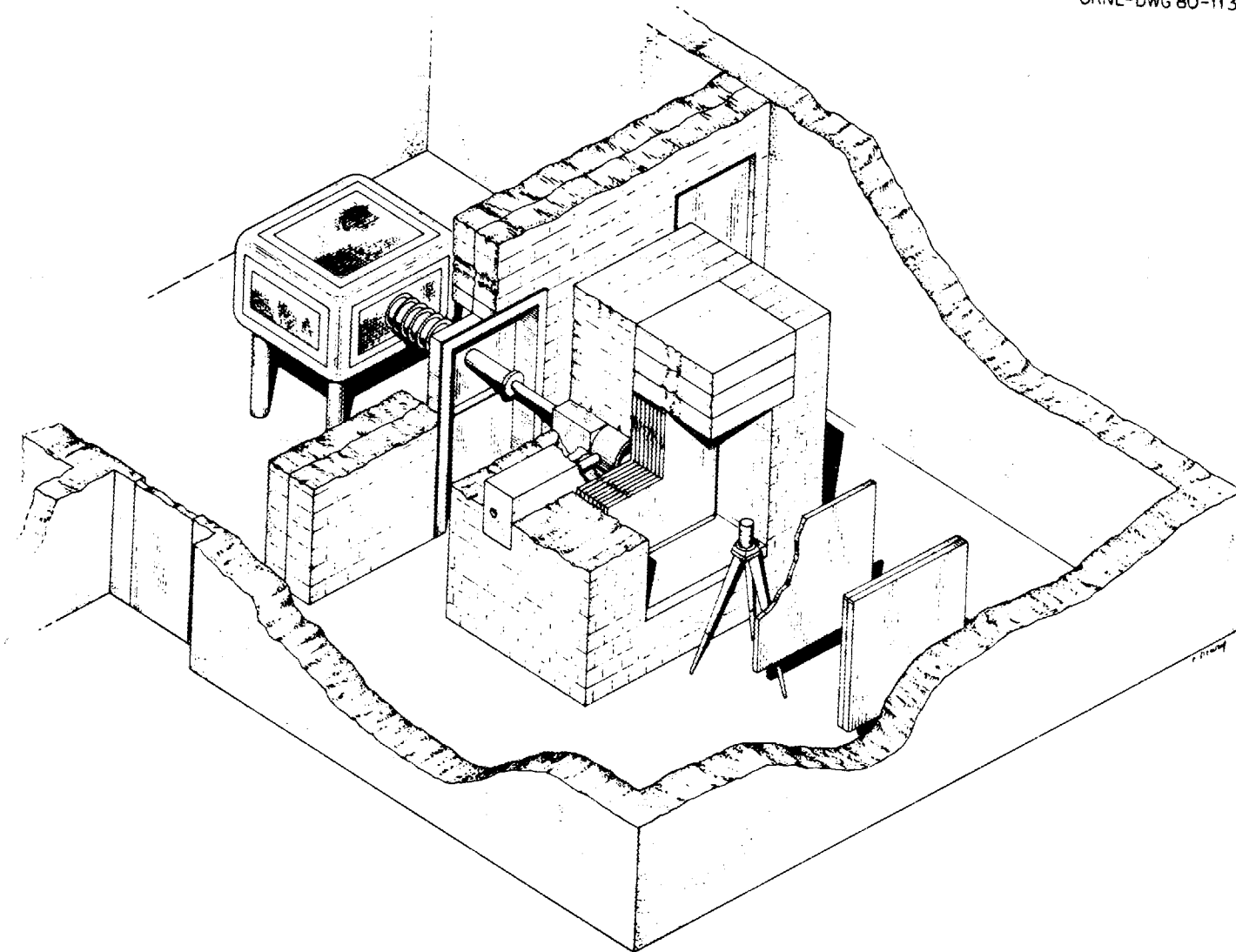


Fig. 1. Artist's rendition of the experimental facility.

via the



fusion reaction. The target consists of 4 mg/cm^2 of titanium-tritide deposited on a 0.254-cm-thick copper disk. The target assembly is enclosed in a cylindrical, re-entrant iron can that is surrounded by concrete which serves as both a shield and a support structure for the shield material slabs.

The iron can that encloses the neutron source has the functions of reflecting the neutrons that are emitted in the backward directions toward the test materials and of softening the neutron spectrum. The neutron spectrum at the mouth of the can, shown in Fig. 2, and, therefore, incident on the test materials, is similar to the first wall neutron spectrum in a fusion reactor. The source can was chosen to be cylindrically symmetric to allow the analysis of the experiment to be carried out in r-z cylindrical geometry. The dimensions of the can were also chosen to provide some collimation of the source neutrons to minimize the spreading of these neutrons in the shields and reduce edge effects that the shields introduce in a cylindrical geometry analysis.

Neutrons and gamma rays transmitted through the shield materials were detected in 66.1 g of NE-213 liquid scintillator contained in a cylindrical aluminum can having a wall thickness of $4.32 \times 10^{-2} \text{ cm}$ and coated on the inside with titanium oxide paint. The active volume of the detector is 79 cm^3 (4.658 cm dia. x 4.658 cm high). The scintillator is mounted on an RCA 8850 photomultiplier tube. Neutron and gamma ray events in the detector were separated using pulse-shape discriminator

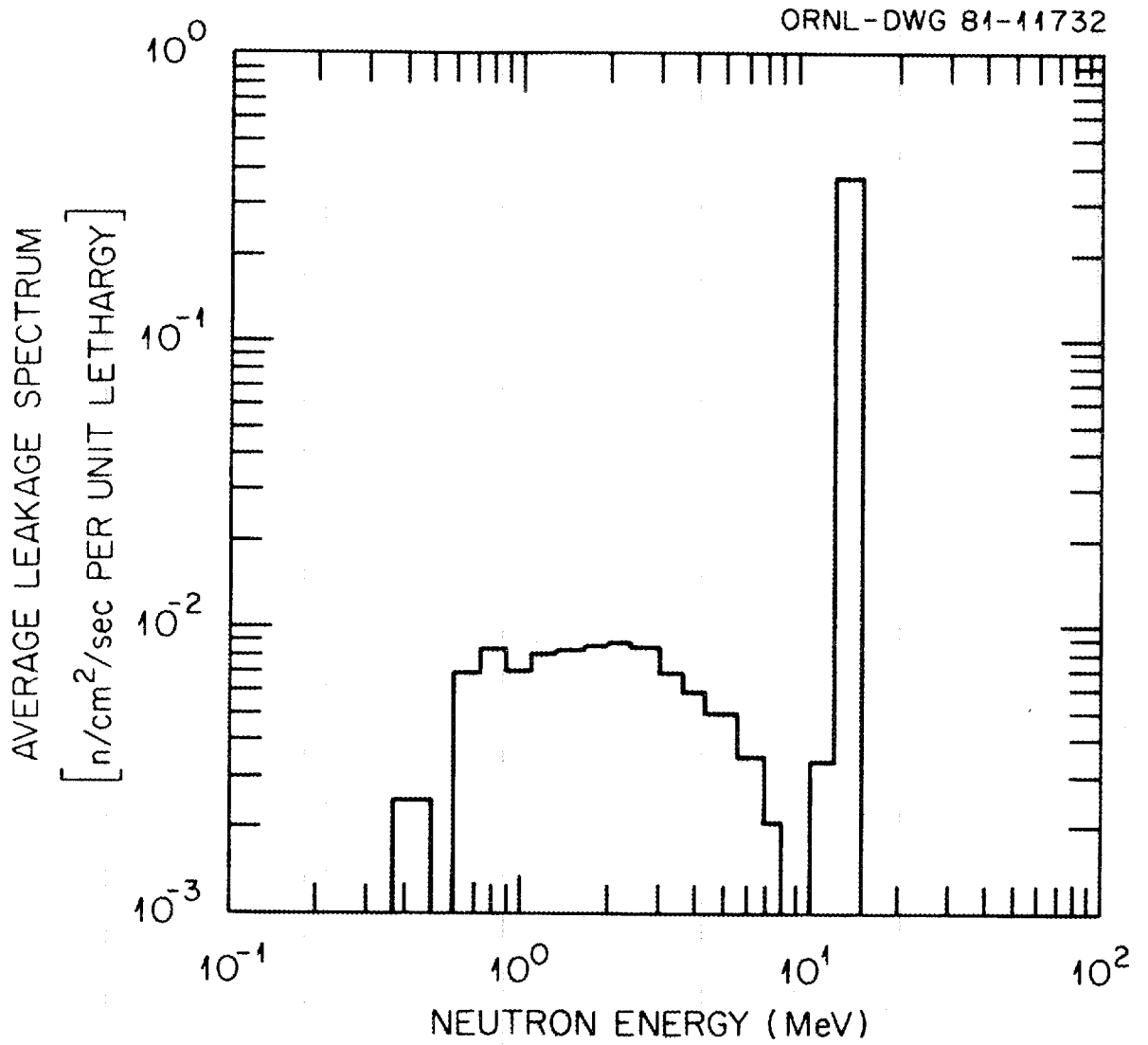


Fig. 2. Neutron Spectrum at the Mouth of the Iron Source Can.

methods and stored in separate memory locations in an ND-812 pulse-height analyzer/computer. The measured spectra are normalized to the absolute neutron yield from the target which was determined using associated particle counting methods.

For 250 keV incident deuterons, the neutrons from the D-T reaction are emitted isotropically in the center-of-mass system. The alpha particles produced in the reaction are emitted at 180° with respect to the neutron so that if the alpha particles are counted within a well-defined solid angle, the number of conjugate neutrons is known and the total neutron source strength can be determined from the kinematics of the reaction.

The NE-213 can effectively detect neutrons with energies above 850 keV and gamma rays with energies above 750 keV. The dynamic range of the neutron pulse-height distribution and the nonlinearity of light output from the scintillator limits the detection of neutrons to those with energies above 850 keV. Although a somewhat broader energy range is possible for gamma rays, (because of the linear response to gamma rays) the energy threshold was fixed at 750 keV. Neutron and gamma ray pulse-height spectra were unfolded using the program FERD⁵ to produce energy spectra. The energy resolution of the detector is given by

$$R_N = [300 + 800/E_N]^{1/2} \quad (2)$$

for neutrons of energy E_N and as

$$R_\gamma = [170 + 288/E_\gamma]^{1/2} \quad (3)$$

for gamma rays of energy E_γ . R_N and R_γ are the full width at half-maximum (in percent) of the detector response to neutrons and gamma rays.

A. Experimental Facility Shield Design Calculations

The design of the experimental facility, and, in particular, the concrete test slab support/shield was supported by two-dimensional analyses to estimate the background radiation levels as a function of the shield design and to minimize their radiation levels by optimizing the experiment configuration. The experimental room was modelled for the calculations using the geometry shown in Fig. 3. The experimental components were represented in r-z geometry with cylindrical symmetry about the deuteron beam axis.

To determine acceptable radiation levels for the planned attenuation experiments, a maximum attenuation experiment was conceived for the purpose of analysis. In this experiment, the transmission of fast neutrons and gamma rays through 1 m of SS-304 would be measured. Incorporating a 1-m-thick SS-304 shield attenuates the fast neutron flux by eight orders of magnitude. A large portion of the epithermal portion of the neutron flux, however, escapes from the shield and contributes to the room background. The concrete shield surrounding the 1-m-thick SS-304 must then be adequately designed to allow $\lesssim 10\%$ background levels for both the fast neutron (>850 keV) and gamma ray (>750 keV) measurements. If these conditions are assured for this setup, then the foreground-to-background ratios will be acceptable in the planned experiments wherein the test shield thicknesses are less than 1 m thick.⁴

The shield design calculations were carried out using the two-dimensional radiation transport code DOT⁶ incorporating a 45-neutron,

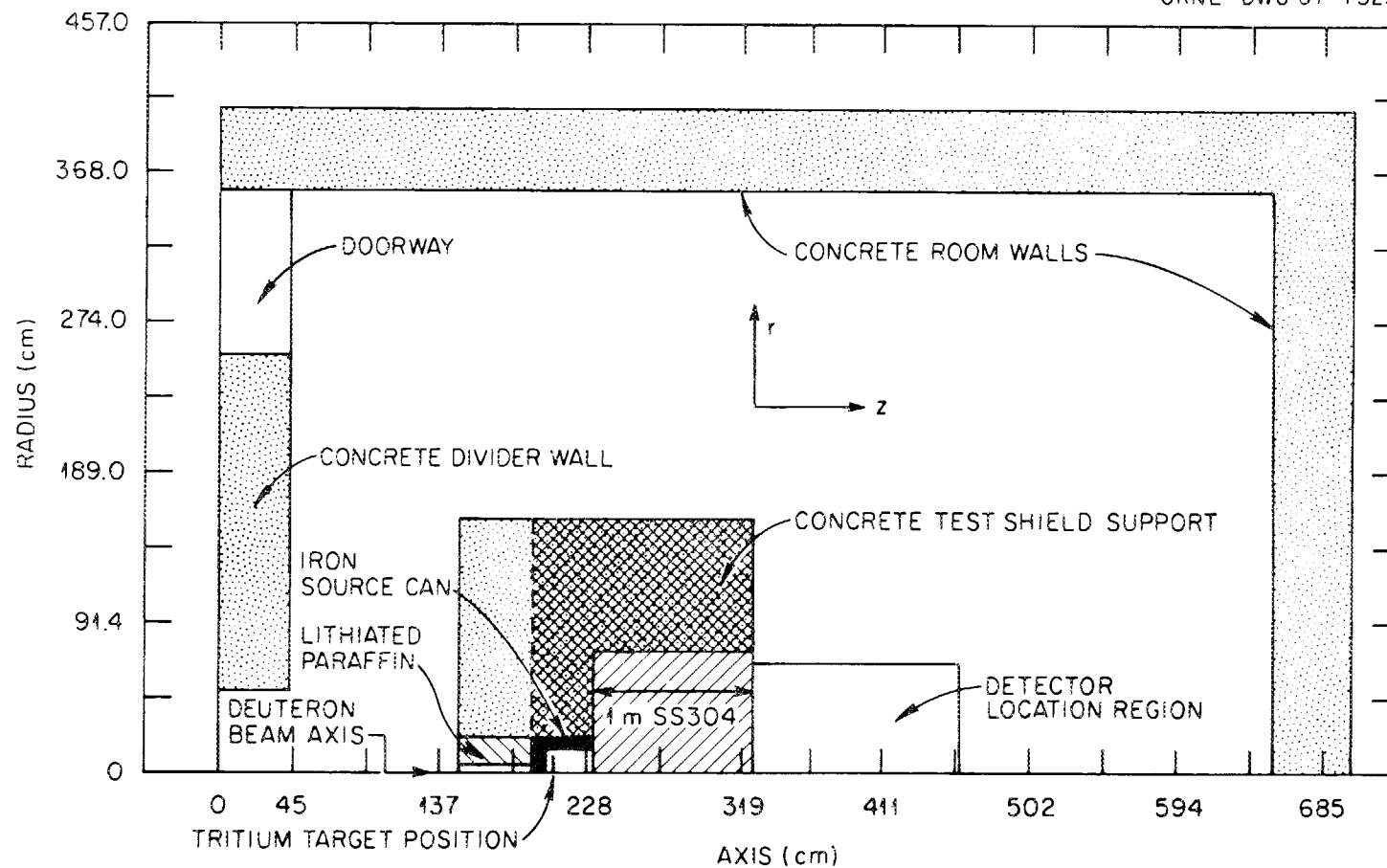


Fig. 3. Two-dimensional calculational model of the full room geometry.

16-gamma-ray energy group transport cross section library with the scattering cross sections represented in a P_3 Legendre expansion.⁷ An initial series of calculations performed for the concrete support/shield configuration and thickness indicated by the cross-hatched area in Fig. 3. Figures 4 and 5 show the results of the DOT calculations in the form of isoflux contours of the anticipated total and fast neutron and gamma ray fluxes in the experimental room. These data, as well as the remainder of the isoflux contours given in this section, are for a 14-MeV D-T neutron source strength of 1 n/s.

It is clear from these initial results that a significant background problems exists behind the stainless steel shield where the measurements would be made. The neutron flux background is primarily due to source neutrons streaming out the back of the iron source can and around the back and sides of the facility shield. Most of the gamma rays on the other hand arise from fast neutron thermalization and capture in the concrete walls of the room and facility shield, as well as from background thermal neutrons being captured at the back face of the stainless steel experimental shield.

To counteract these effects, several modifications were made to the facility shield. First, additional concrete was placed at the back end of the shield to reduce the amount of radiation streaming around the shield. The results of transport calculations for the total and fast neutron fluxes in this configuration showed that streaming around the shield was reduced, but not enough to reduce the background contribution at the detector position to acceptable levels. The major remaining portion of the streaming was due to neutrons streaming directly out of the hold in the

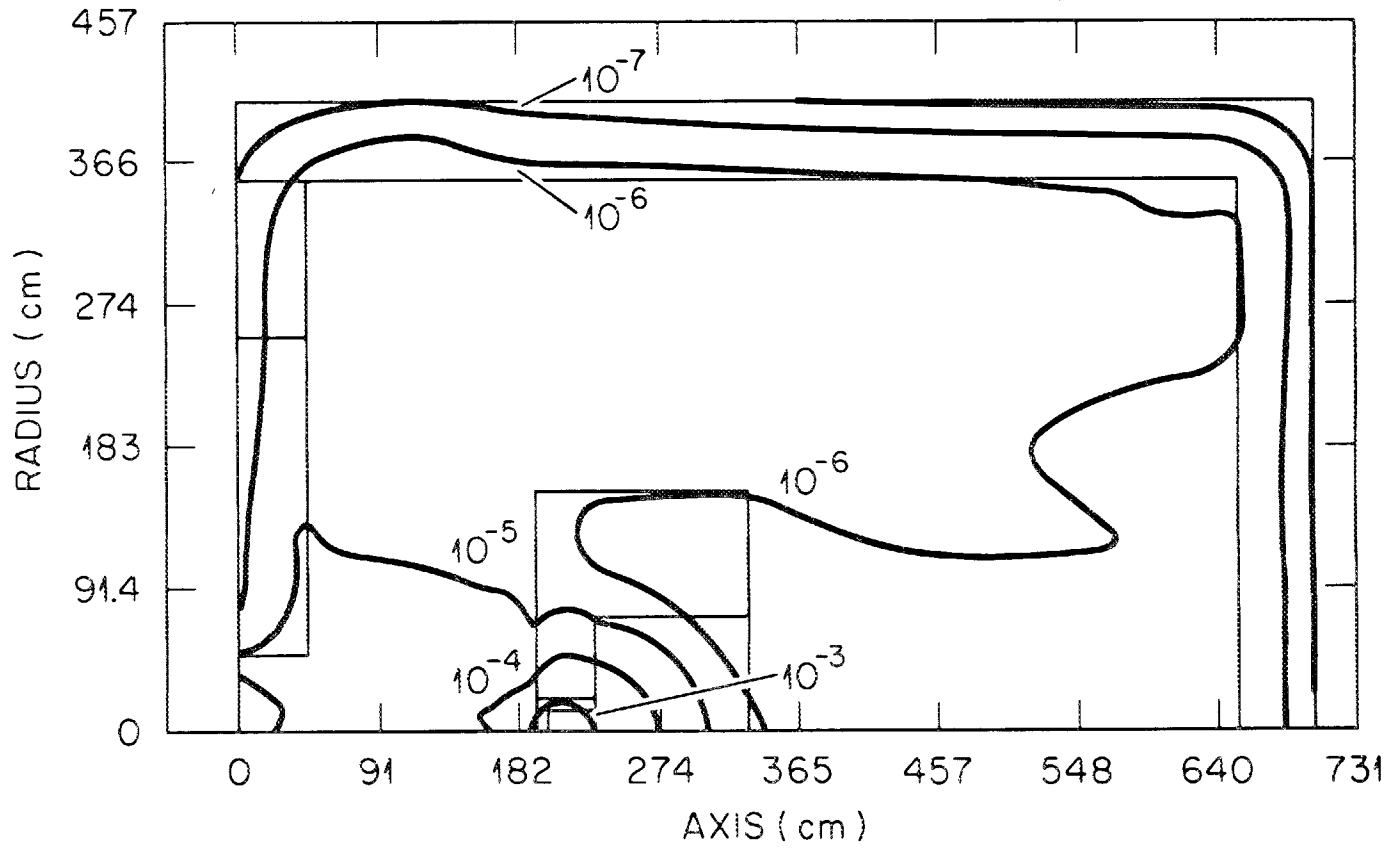


Fig. 4. Iso-flux contours ($n/cm^2/s$) for the total neutron flux in the preliminary experimental facility design. Data are normalized to a 14 MeV neutron source strength of 1 n/s.

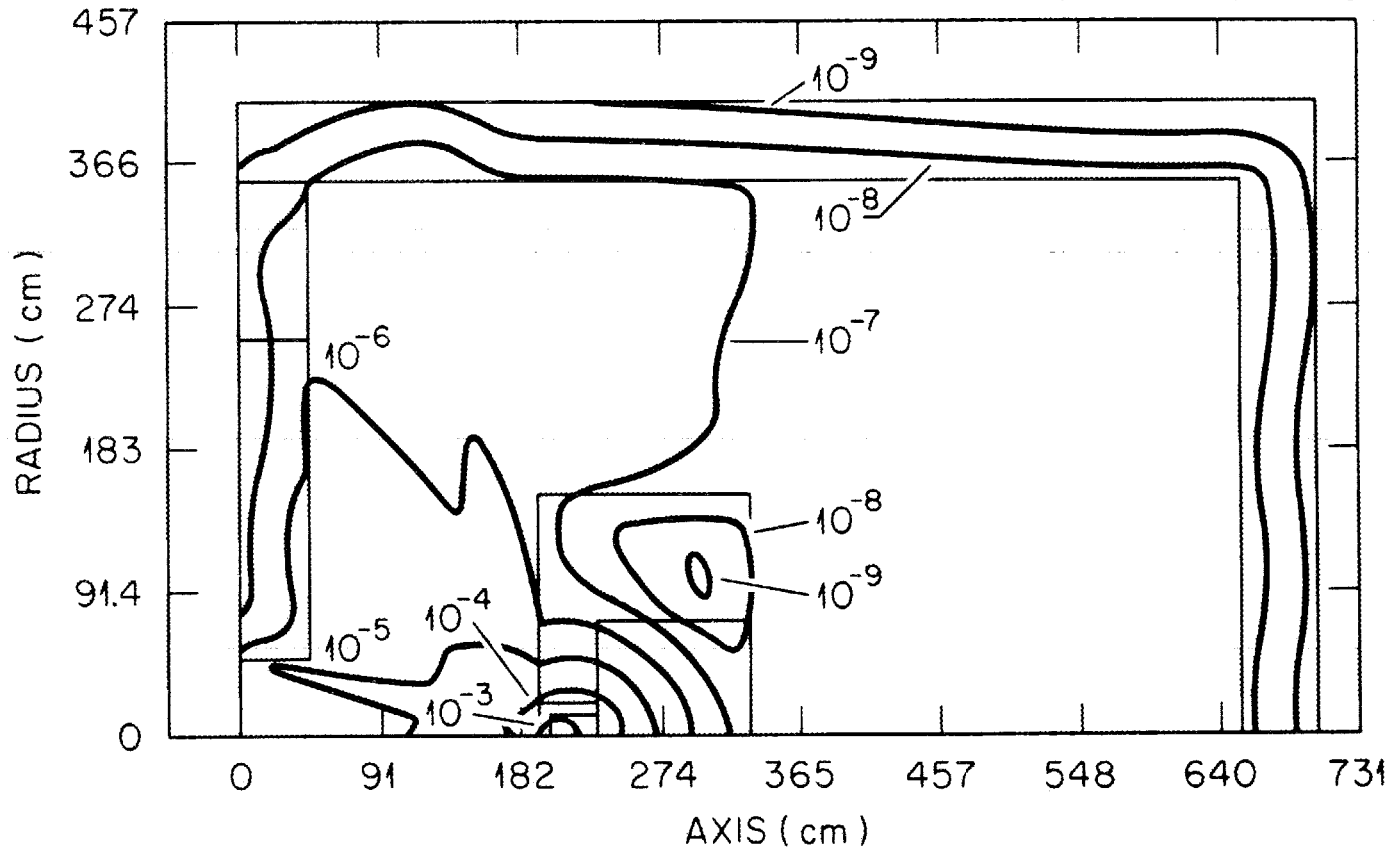


Fig. 5. Iso-flux contours ($n/cm^2/s$) for the neutron flux above 600 keV in the preliminary experimental facility design. Data are normalized to a 14 MeV neutron source strength of 1 n/s.

shield where the deuteron beam drift tube enters the iron cavity.

To eliminate this problem, a lithiated-parrafin shielding plug was designed to fit the beam entrance hole. This shield is light and movable to allow access to the iron can for periodic replacement of the tritium target. Figures 6 and 7 show the significant reductions in the total and fast neutron streaming achieved with these design modifications. The flux contours now indicate an order of magnitude less background at the detector position and it appears that the desired fast neutron background level is now below 10%. The additional concrete and the lithiated-parrafin plug are also shown in Fig. 3.

Inspection of Figs. 8 and 9 which show the thermal neutron and fast gamma ray components of the radiation field indicated, however, that further problems would arise from the high thermal neutron background. This component itself would not be a problem if only fast neutron measurements were to be made, but since gamma ray fluxes are also of interest, the thermal neutrons might produce significant background gamma ray flux levels through capture in the facility shield, room walls, and at the face of the last experimental shield slab. These background gamma rays could mask the source of gamma rays from capture and inelastic scattering in the experimental shield which needs to be measured. In the hypothetical maximum attenuation experiment the thermal background is clearly not a problem (i.e., 10^{-8} n/cm²·s for the total flux). The gamma-ray curves (Fig. 9) bear this out, with the source of the gamma rays being epithermal neutrons in the experimental shield (i.e., compare Figs. 4 and 9).

The contours in Fig. 8, however, do indicate a potential problem in that the 10^{-8} n/cm²·s thermal flux at the end of the shield is due to

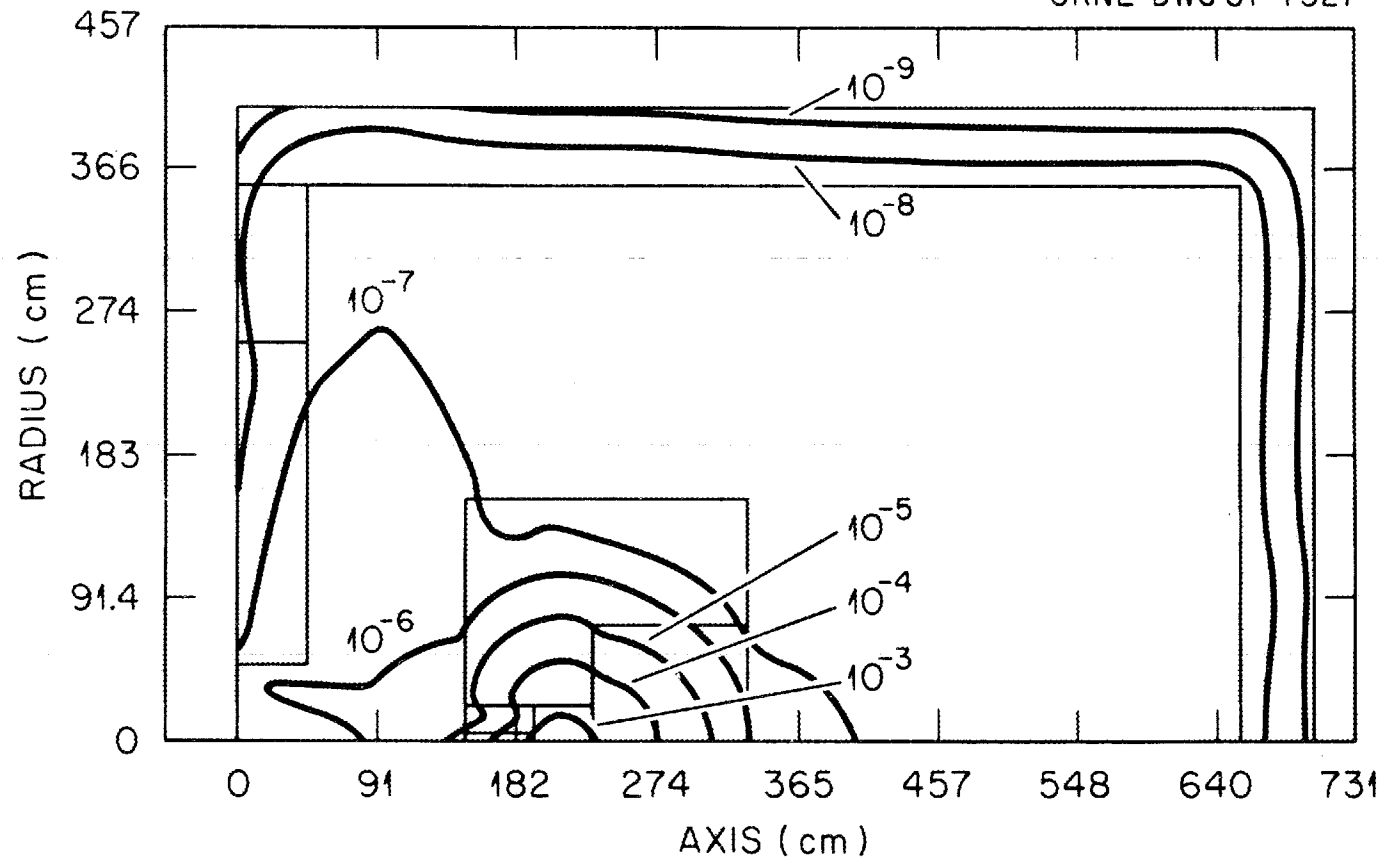


Fig. 6. Iso-flux contours ($\text{n}/\text{cm}^2/\text{s}$) for the total neutron flux in the revised experimental facility design. Data are normalized to a 14 MeV neutron source strength of 1 n/s.

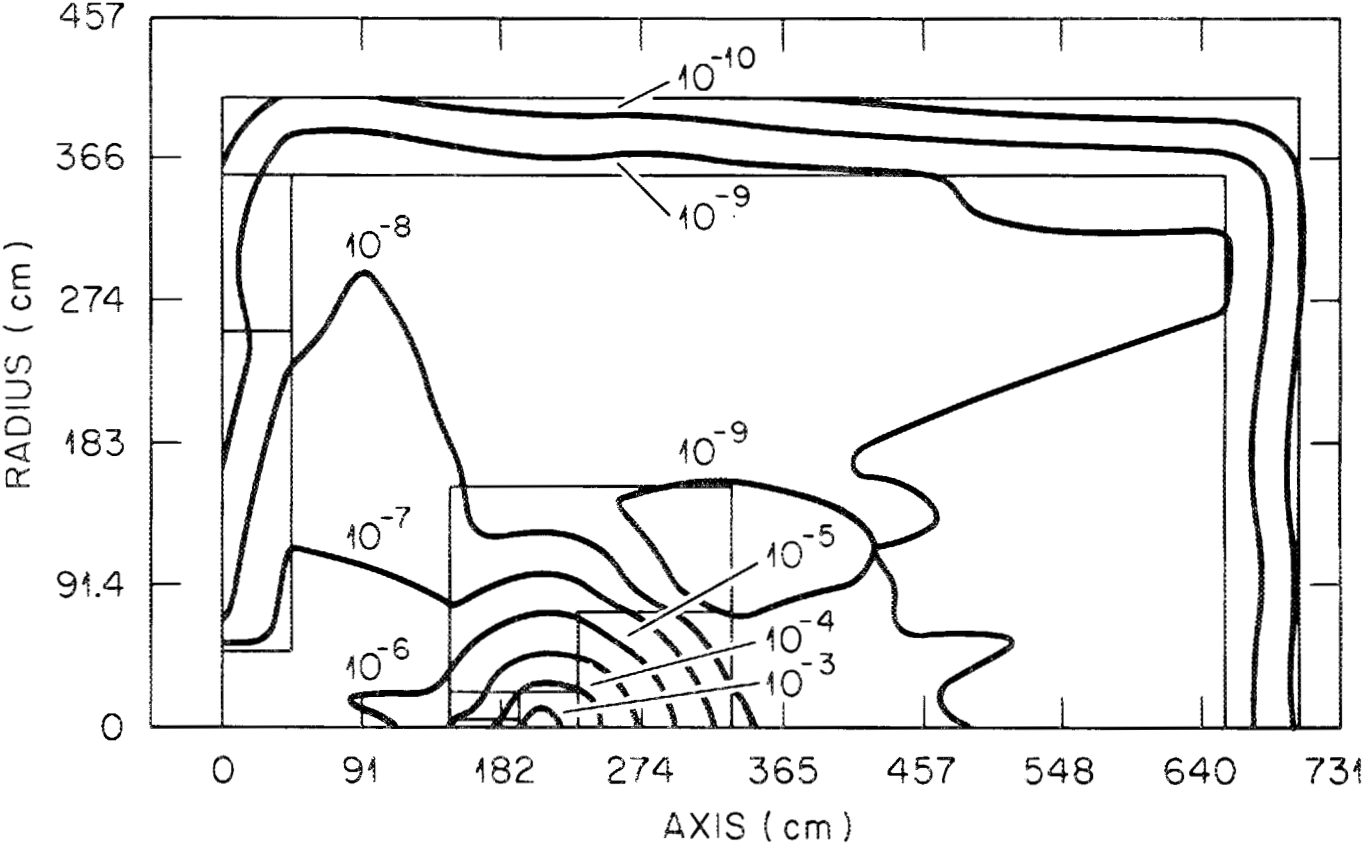


Fig.7. Iso-flux contours ($n/cm^2/s$) for the neutron flux above 600 keV in the revised experimental facility design. Data are normalized to a 14 MeV neutron source strength of 1 n/s.

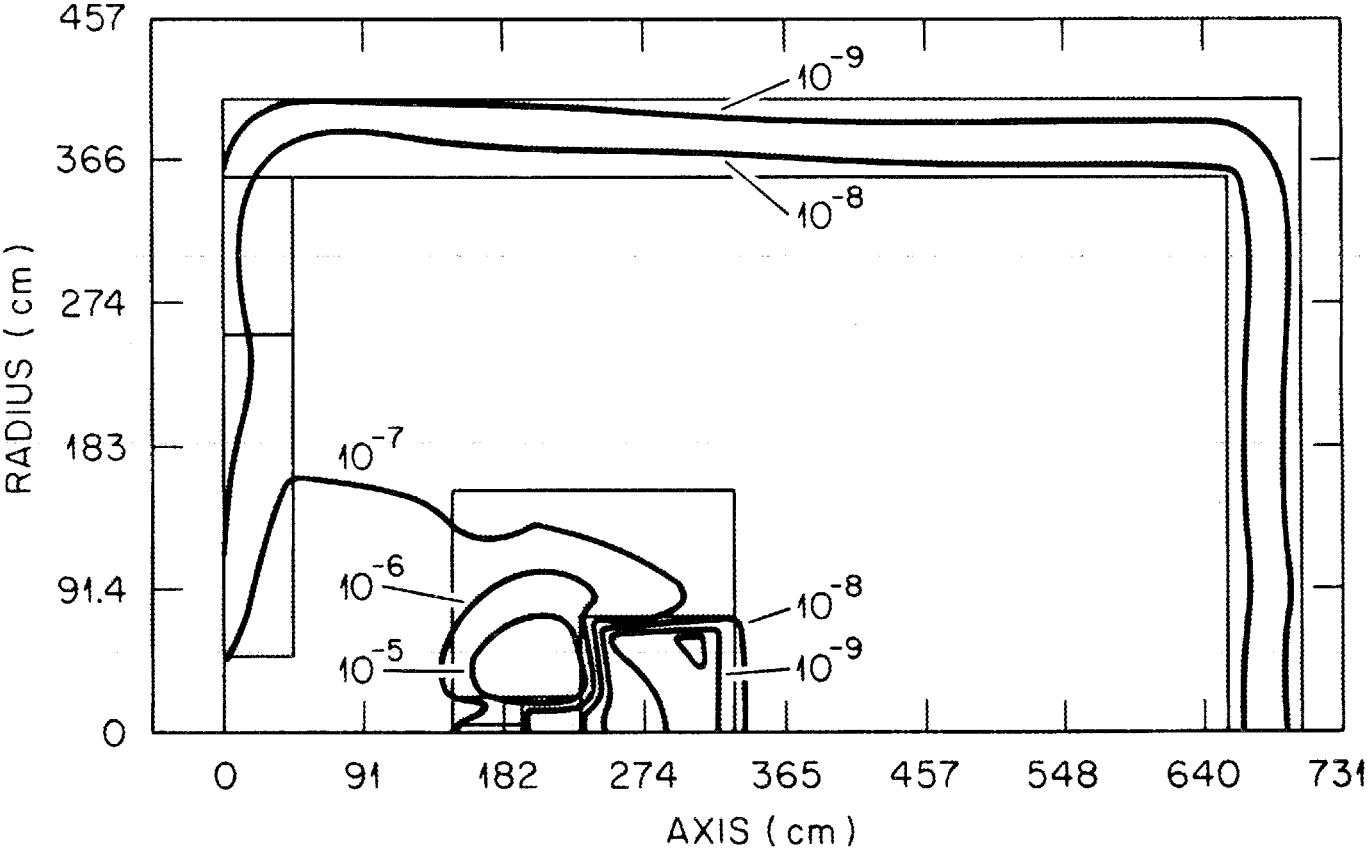


Fig. 8. Iso-flux contours ($n/cm^2/s$) for the thermal neutron flux in the revised experimental facility design. Data are normalized to a 14 MeV neutron source strength of 1 n/s.

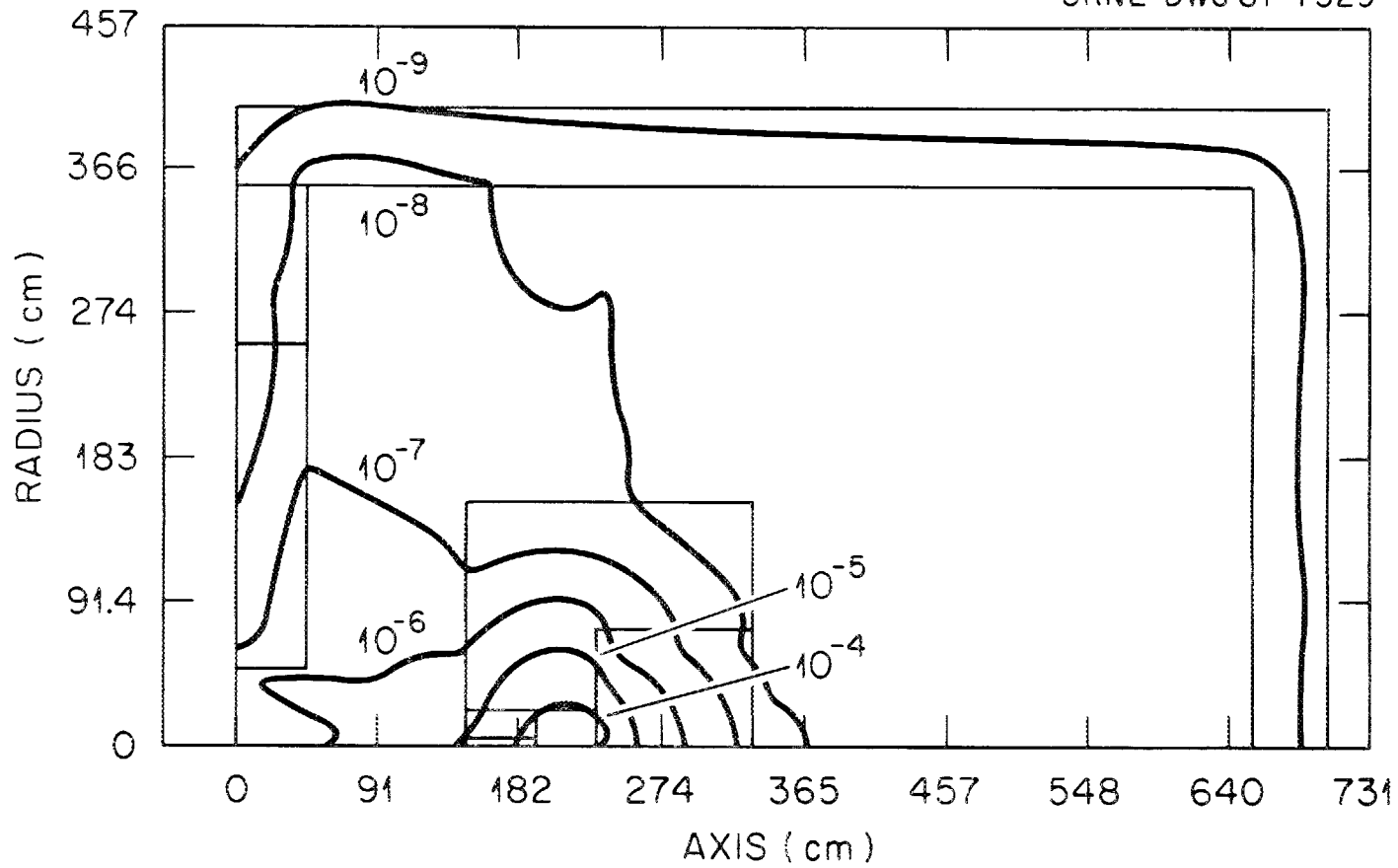


Fig. 9. Iso-flux contours ($\gamma/\text{cm}^2/\text{s}$) for the gamma ray flux above 550 keV in the revised experimental facility design. Data are normalized to a 14 MeV neutron source strength of 1 n/s.

room return. It is clear from the contours of thermal neutron flux that a way to alleviate this potential background problem would be to make *in situ* measurements of the fast neutron and gamma ray fluxes at a position inside the shield. Several centimeters inside the shield, the background gamma ray fluxes arising from outside the experimental shield would be attenuated sufficiently to insure the dominance of the gamma ray component penetrating through the shield from the source. To maintain greater freedom of movement and ease of measurement a thermal neutron shield was added behind the experimental shield.

Calculational results for two thicknesses of the proposed thermal shield (7.5 cm and 15 cm) led to the design of a minimum 10 cm stainless steel configuration which would provide more than an order of magnitude attenuation of any thermal neutron source in the walls directly behind the shield. Results of thermal neutron flux calculations for the hypothetical experiment indicate that no significant reductions are achieved in the thermal neutron background levels arising from sidewall contributions (the major source of thermals in this case) but then again these levels were well below what would constitute a problem to begin with. In any event, the thermal shield acts in two ways: 1) it further attenuates fast neutrons transmitted through the experimental shield before they reach the concrete walls of the room directly behind the shield and thermalize, and 2) it significantly attenuates thermal neutrons produced in the wall behind the shield, effectively preventing them from reaching the face of the experimental configuration where they would create gamma rays when captured. This modification insures that both neutrons and gamma rays produced in the shield can be measured without significant

background sources.

The results of the transport analysis obtained using the revised geometry are shown in the isoflux contour plots in Figs. 10-13. These data show that the background radiation levels will be $\sim 10\%$ in the proposed attenuation experiments.

B. Optimization of the Computational Model

In order to minimize the computing time in the analysis of the radiation transport in the various experimental shield configurations, the total room geometry shown in Fig. 3 was reduced to the smaller, but equivalent, geometry. The geometry shown in Fig. 3 including the 10-cm-thick thermal shield (see, for example, Fig.10) requires 76 radial and 92 axial mesh intervals to describe the various components. If the geometry can be reduced and still reproduce the flux contours in the vicinity of the detector location, considerable savings in computation time and core storage can be realized.

The calculational geometry was reduced by replacing the room walls by albedo surfaces having a reflection factor of 0.20 for all energy groups and relocating these surfaces along the radial boundary of the concrete support/shield. Also, the rear wall of the room was relocated in the model by placing it immediately behind the thermal neutron shield. Results of transport calculations obtained using this geometry (which is now described using 42 radial and 82 axial mesh intervals) are shown in the form of isoflux contours in Figs. 14 and 15.

The isoflux contours of the neutron flux above 600 keV and the gamma ray flux above 550 keV shown in Figs. 14 and 15, respectively, agree very favorably with the corresponding data shown in Figs. 11 and 13,

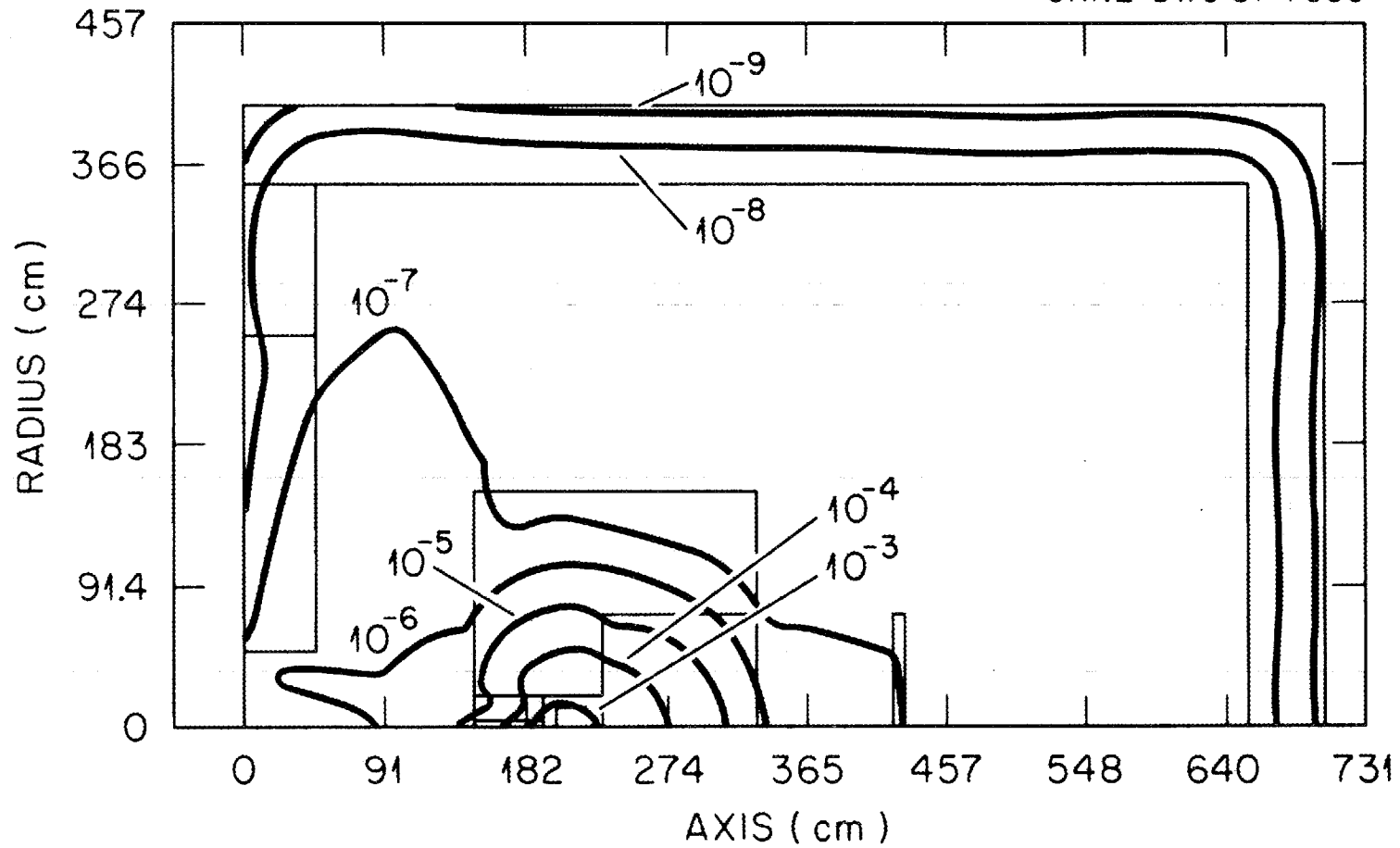


Fig. 10. Iso-flux contours ($n/cm^2/s$) for the total neutron flux in the final experimental facility design. Data are normalized to a 14 MeV neutron source strength of 1 n/s.

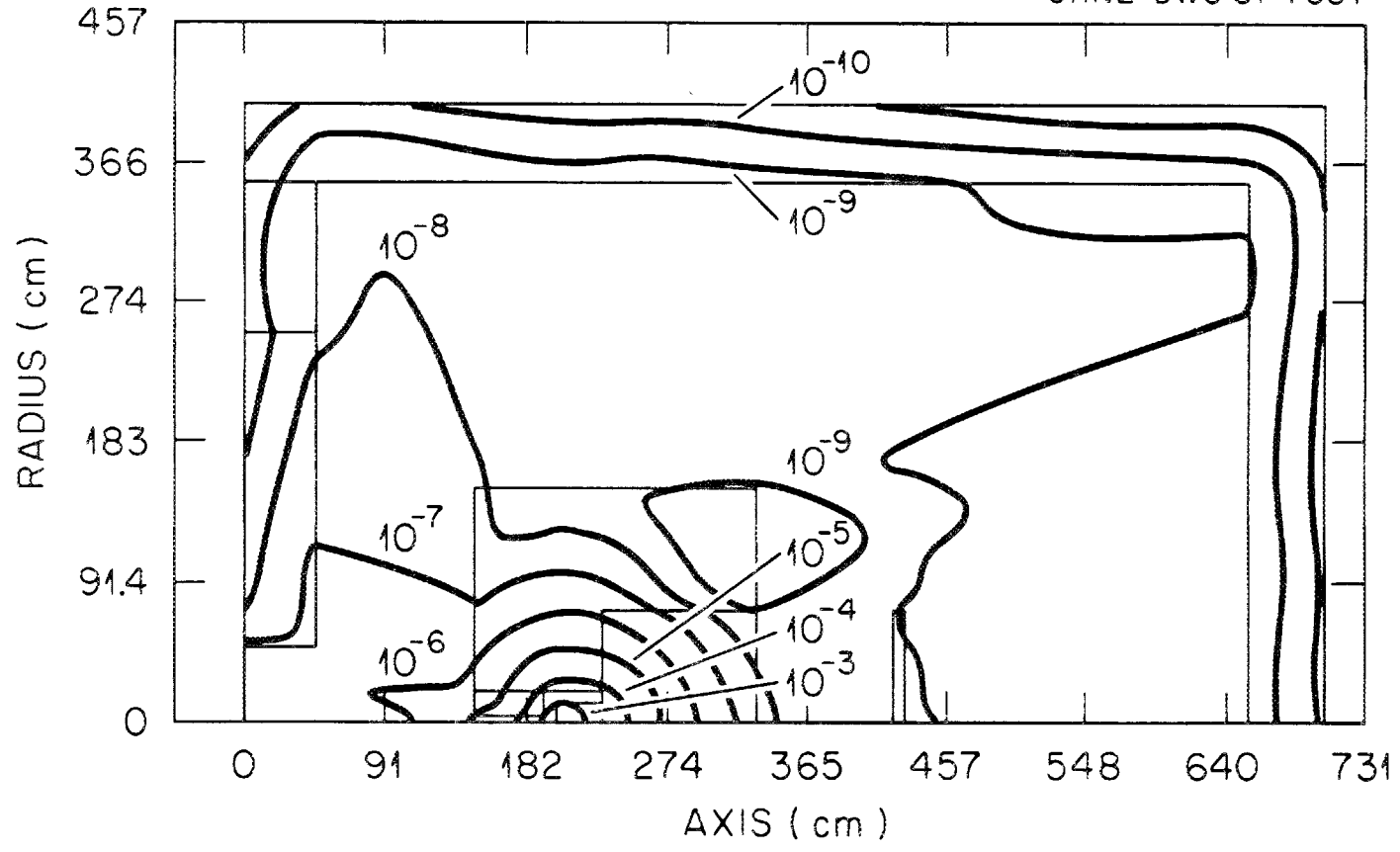


Fig. 11. Iso-flux contours ($n/cm^2/s$) for the neutron flux above 600 keV in the final experimental facility design. Data are normalized to a 14 MeV neutron source strength of 1 n/s.

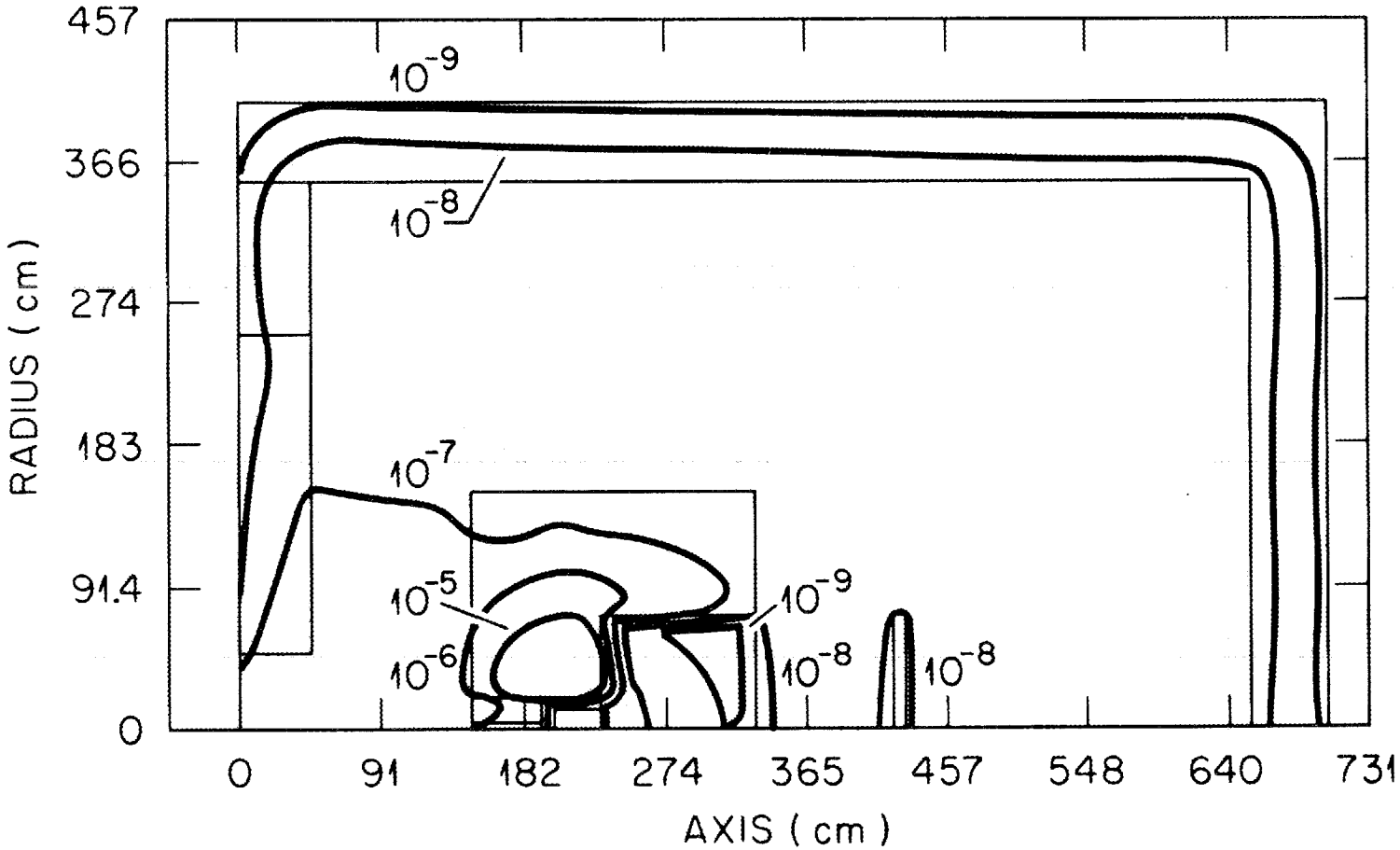


Fig. 12. Iso-flux contours ($n/cm^2/s$) for the thermal neutron flux in the final experimental facility design. Data are normalized to a 14 MeV neutron source strength of 1 n/s.

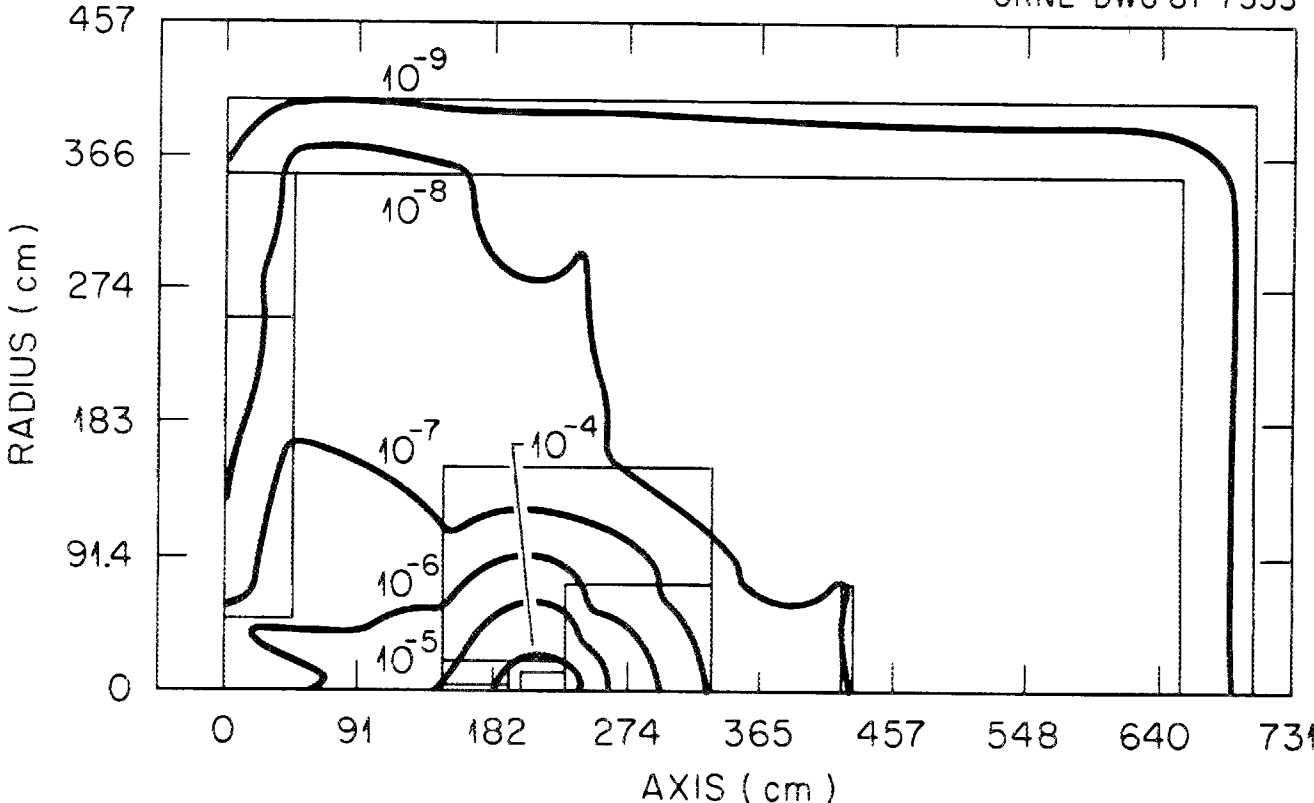


Fig. 13. Iso-flux contours ($\gamma/\text{cm}^2/\text{s}$) for the gamma ray flux above 550 keV in the final experimental facility design. Data are normalized to a 14-MeV neutron source strength of 1 n/s.

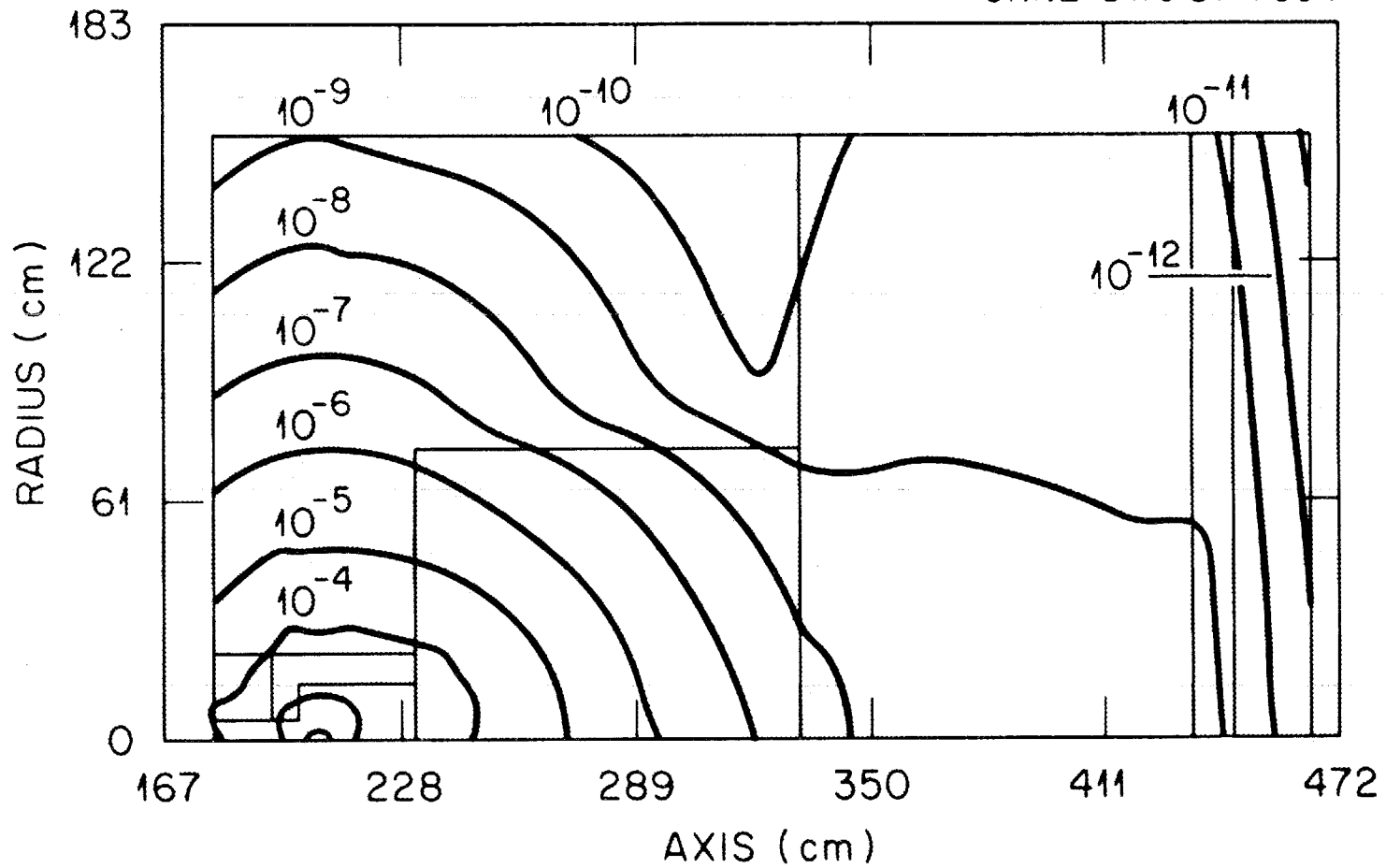


Fig. 14. Iso-flux contours ($n/cm^2/s$) for the neutron flux above 600 keV in the reduced geometry model of the final facility shield. Data are normalized to a 14 MeV neutron source strength of 1 n/s.

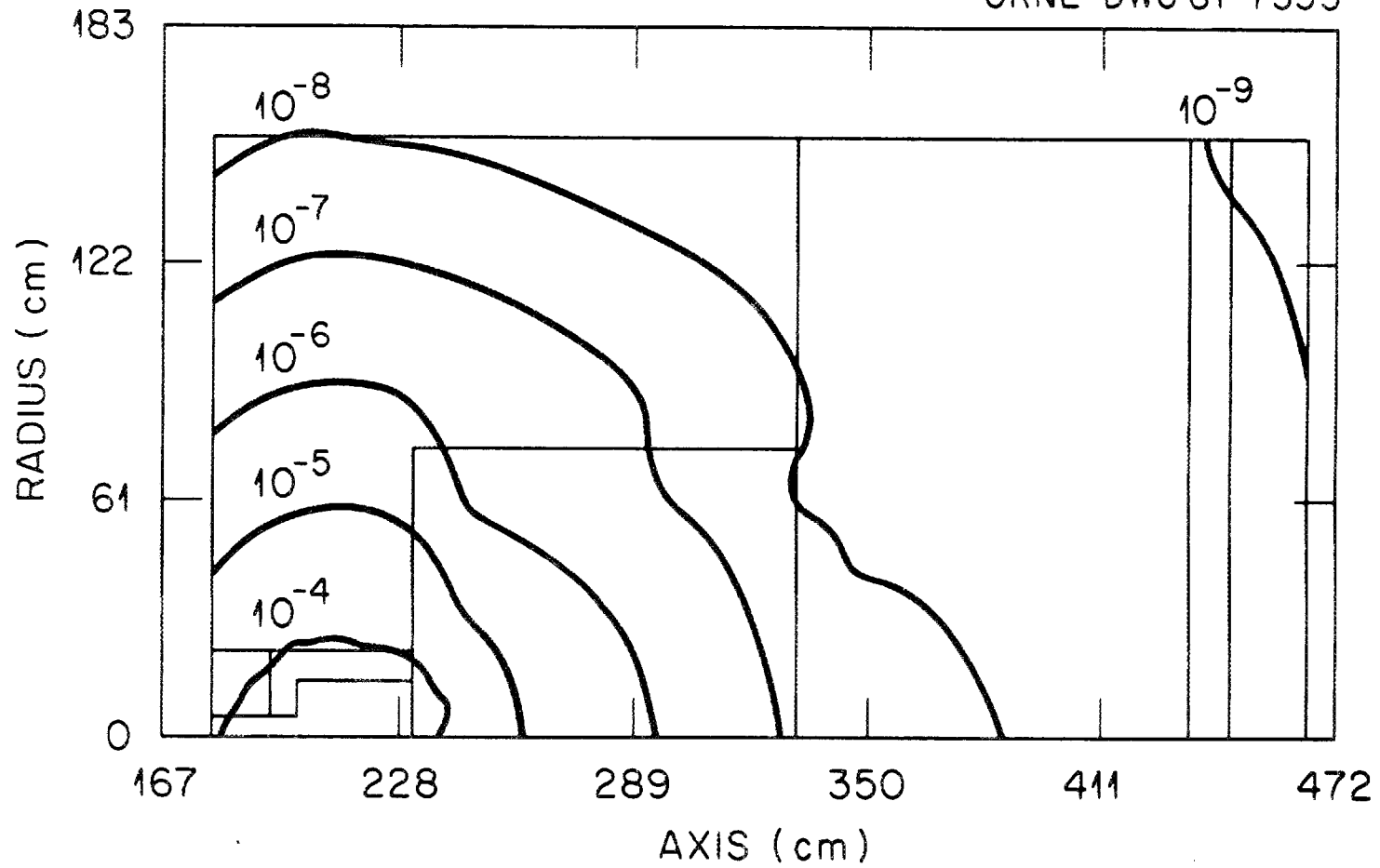


Fig. 15. Iso-flux contours ($\gamma/\text{cm}^2/\text{s}$) for the gamma ray flux above 550 keV in the reduced experimental facility design. Data are normalized to a 14 MeV neutron source strength of 1 n/s.

respectively, obtained for the full room geometry. These comparisons clearly show that the remainder of the room can be neglected and more calculational detail can be placed on the more important parts of the geometry with a reduction in the transport calculation storage requirements and running time.

III. ENERGY ANGLE RELATIONS FOR D-T NEUTRONS

The reactions of 250 keV deuterons in the 4 mg/cm^2 thick titanium tritide target produce neutrons which range in energy from 13.2 to 15.1 MeV depending on the energy at which the deuteron reacts in the target and the angle of emission of the neutron from the target. The neutron angle-energy correlation also depends on the angular differential cross section for the D-T reaction and the kinematics of the reaction. The angle-energy dependence of the neutron distribution must be taken into account in the radiation transport calculations to assure that the measured and calculated data are compared to the same neutron distribution.

The probability, P , that a deuteron of energy E_d will undergo a D-T reaction while traveling a distance, dx , in target containing N_t tritium atoms is

$$P = N_t \int_0^{E_d} \sigma(E_d) dx \quad (4)$$

where $\sigma(E_d)$ is the total cross section for the D-T reaction. The deuteron slows down continuously in the target and $\sigma(E_d)$ is a strong function of the deuteron energy, so Eq. (4) can be re-written

$$P = N_t \int_0^{E_d} \sigma(E_d) dE / (dE/dx) \quad (5)$$

where (dE/dx) is the rate of deuteron energy loss in the target. For deuterons incident on a 4 mg/cm^2 thick target, the rate of energy loss is given by

$$(dE/dx)_{TiT} = 0.9014 (dE/dx)_{Ti} + 0.0986(dE/dx)_T \quad (6)$$

where $(dE/dx)_{Ti}$ and $(dE/dx)_T$ are the stopping powers for deuterons in titanium and tritium, respectively.⁸ These stopping powers are plotted as a function of deuteron energy in Fig. 16. The energy dependence of the angular differential cross section, $\sigma(E_d, \Omega)$, for the D-T reaction is plotted in Fig. 17. These data correspond to

$$\sigma(E_n) = 4\pi\sigma(E_d, \Omega). \quad (7)$$

Therefore, Eq. (5) can now be written

$$P(E_n, \Omega) = \frac{N_t}{4\pi} \int_0^{E_d} \sigma(E_d, \Omega) dE / (dE/dx)_{TiT} \quad (8)$$

which is the probability that a neutron of energy E_n is emitted into solid angle Ω from the reaction of a deuteron of energy E_d in titanium-tritide.

When Eq. (8) is used in conjunction with the kinematic equations for a two-body reaction, the angle-energy dependence of the D-T neutrons is obtained. A computer program was written to perform these calculations and to process the data in a form suitable for input to the transport codes.

The probability distribution function for the emission of neutrons of energy E_n from the interaction of 250 keV deuterons in the target is

ORNL-DWG 81-7336

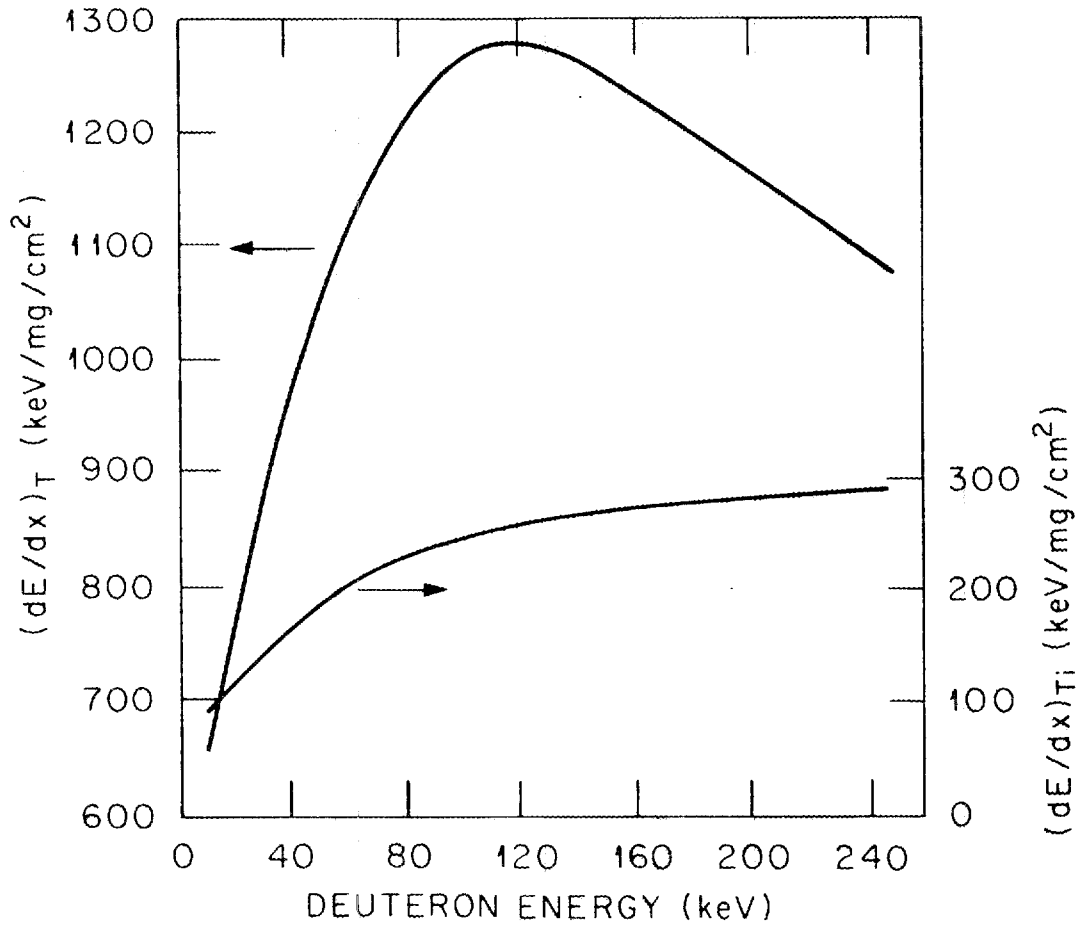


Fig. 16. Stopping power for deuterons in T and Ti vs. deuteron energy.

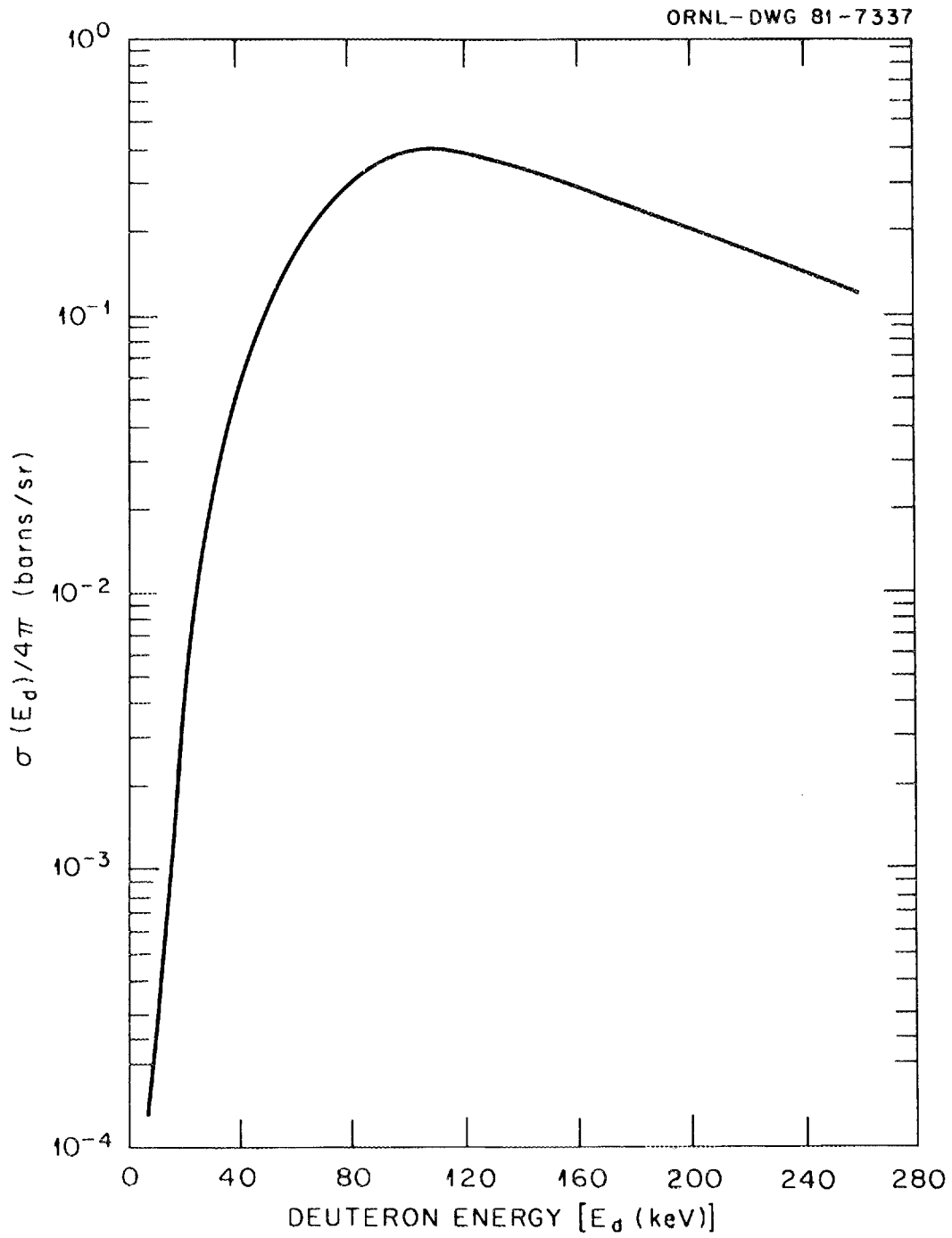


Fig. 17. Differential cross section for the $T(D,n)^4\text{He}$ reaction vs. deuteron energy.

shown for two energy group structures in Table I. The probabilities are given in the energy group structure of the BUGLE data set⁷ and an energy group structure having a finer mesh structure in the energy interval in which neutrons are emitted. These data indicate that the energy group

Table I. Probability for the Emission of Neutrons of Energy E_n Versus Neutron Energy Interval

Bugle Energy Group Structure		Modified Energy Group Structure*	
Energy Interval (MeV)	$P(E_n)$	Energy Interval (MeV)	$P(E_n)$
17.333-14.918	0.0130	17.333-15.683	0.0
14.918-14.191	0.4227	15.683-14.918	0.0130
14.191-13.499	0.5001	14.918-14.550	0.1599
13.499-12.840	0.0642	14.550-14.191	0.2678
		14.191-13.840	0.2913
		13.840-13.499	0.2088
		13.499-12.840	0.0642
Total	1.0000		1.0000

*Details of the procedure used to obtain this energy group structure and the concomitant transport cross section library are given in Sec. IV.

structure used in the BUGLE library is too coarse to represent the energy distribution of the D-T neutrons. For example, this group structure shows that neutrons can be emitted with energies as high as 17.33 MeV which is beyond the energy that is kinetically possible. Also, neutrons can be

emitted with nearly equal probability in the energy interval between 13.499 and 14.918 MeV. To obtain a more accurate description of the neutron source term, the group structure was revised as shown in the right-hand side of the table. In the revised group structure, the maximum neutron energy is 15.683 MeV which more nearly duplicates the maximum allowed neutron energy of 15.1 MeV. The finer group structure between 13.499 and 14.918 MeV yields a more accurate description of the neutron distribution. Both the BUGLE and the revised energy group structures are subsets of the VITAMIN C energy group structure⁹ from which the radiation transport cross sections were derived. Detailed discussions of the procedures used to generate the cross section libraries in the appropriate energy group structure are given in Section IV.

The angle-energy distribution was obtained for neutrons emitted into the polar angular intervals of 0-40, 40-90, and 90-180 degrees. Uniform neutron emission into azimuthal angles was assumed. The angular interval of 0-40 degrees was chosen since this interval corresponds to that defined by neutrons emitted out of the mouth of the source can. (See Fig. 3) The angular intervals of 40-90 and 90-180 degrees account for neutron emission through the "side" of the concrete support/shield and neutron emission into the "backward" directions, respectively. The probability for neutron emission into the specified angular intervals as a function of energy from the reactions of 250 keV deuterons in a 4 mg/cm² thick titanium-tritide target are summarized in Table II.

Table II. Angle-Energy Dependence of Neutron Emitted from the $T(D,n)^4\text{He}$ Reaction

Energy Interval (MeV)	$E_d = 250 \text{ keV}$		
	0°-40°	Angular Interval 40°-90°	
			90°-180°
15.68-14.92	0.0130		
14.92-14.55	0.0920	0.0697	
14.55-14.19	0.0168	0.2460	
14.19-13.80		0.0750	0.2163
13.80-13.50			0.2088
13.50-12.84			0.0642

IV. NUCLEAR DATA PROCESSING

The analysis of the experimental configuration and the background radiation levels in the experimental room discussed in Section II were carried out using the BUGLE cross section library.⁷ While this data set is adequate for a variety of radiation transport problems, including those discussed in Section II, the requirement for describing the source neutron energy distribution with a finer energy group structure necessitated the construction of a more appropriate radiation transport cross section library.

A new cross section library having 53 neutron and 21 gamma ray energy groups was created. The energy boundaries, which are subsets of those in the VITAMIN C data set, are given in Table III. The energy group structure differs from that of BUGLE by the addition of seven neutron groups between 10- and 15-68 MeV and by the addition of one group between 0.742 and 0.862 MeV. The gamma ray energy group structure is similar to that used in the DLC-37 (100n-21 γ) cross section library¹⁰ but with the lower energy boundary of the 19th energy group at 0.60 MeV rather than 0.40 MeV.

The 53-neutron-21-gamma-ray library was collapsed from the 171-neutron-36-gamma-ray VITAMIN C library. The AMPX system¹¹ was used to generate the working library data. The nuclides comprising the library were self-shielded assuming a homogeneous mixture of concrete. The self-shielded

Table III. 53-Neutron, 21-Gamma-Ray Energy Radiation
Transport Cross Section Group Structure

Neutron Group	Upper Energy (eV)	Neutron Group	Upper Energy (eV)	Gamma Ray Group	Upper Energy (MeV)	
1	0.17333E + 08	28	0.60810E + 06	54	1	14.0
2	0.15683E + 08	29	0.49787E + 06	55	2	12.0
3	0.14918E + 08	30	0.36883E + 06	56	3	10.0
4	0.14550E + 08	31	0.29850E + 06	57	4	8.0
5	0.14191E + 08	32	0.29720E + 06	58	5	7.5
6	0.13840E + 08	33	0.18316E + 06	59	6	7.0
7	0.13499E + 08	34	0.11109E + 06	60	7	6.5
8	0.12840E + 08	35	0.67379E + 05	61	8	6.0
9	0.12214E + 08	36	0.40868E + 05	62	9	5.5
10	0.11052E + 08	37	0.24788E + 05	63	10	5.0
11	0.10000E + 08	38	0.23579E + 05	64	11	4.5
12	0.90484E + 07	39	0.15034E + 05	65	12	4.0
13	0.81873E + 07	40	0.91188E + 04	66	13	3.5
14	0.74082E + 07	41	0.55308E + 04	67	14	3.0
15	0.60653E + 07	42	0.33546E + 04	68	15	2.5
16	0.49659E + 07	43	0.20347E + 04	69	16	2.0
17	0.40657E + 07	44	0.12341E + 04	70	17	1.50
18	0.36788E + 07	45	0.74852E + 03	71	18	1.0
19	0.27253E + 07	46	0.45400E + 03	72	19	0.60
20	0.23653E + 07	47	0.27536E + 03	73	20	0.20
21	0.23069E + 07	48	0.16702E + 03	74	21	0.10
22	0.22313E + 07	49	0.10130E + 03			0.010
23	0.16530E + 07	50	0.61442E + 02			
24	0.13534E + 07	51	0.37267E + 02			
25	0.86294E + 06	52	0.10677E + 02			
26	0.82085E + 06	53	0.41399E + 00			
27	0.74274E + 06		0.10000E - 04			

neutron interaction AMPX interface generated using the BONAMI module was processed in the CHOX module along with photon production and interaction interfaces to form a combined neutron gamma ray interface. These data were processed by NITAWL to convert the data to a coupled, P_3 library (171n-36 γ) which is suitable for input to the ANISN code¹² which collapses the cross sections to the 51-neutron-21-gamma-ray energy group structure.

The cross sections were collapsed in the following manner. The two-dimensional model used to describe the experimental configuration was divided into three regions defined by the polar angular intervals of 0° - 40° , 40° - 90° , and 90° - 180° as shown in Fig. 18. The angular intervals were measured relative to the axis of cylindrical symmetry with the D-T neutron source as the vertex. Azimuthal symmetry was assumed. Each angular region defined in the two-dimensional geometry was then modeled in spherical geometry preserving, insofar as possible, the order and dimensions of the materials in the angular interval. Three separate ANISN calculations were then performed to collapse the fine group (171n-36 γ) cross sections for the materials defined in each sphere. The procedure is shown in the block diagram in Fig. 19.

The 171-neutron-36-gamma-ray energy group master cross section data from the AMPX system served as input to the processing code AXMIX.¹³ This code mixes the nuclides according to the compositions of the materials in the experiment.

The compositions are given in Table IV. ANISN calculations were carried out for each sphere using the neutron energy distribution for the angular interval represented by the sphere (see Table II) as the neutron source term. Three collapsed (53n-21 γ) group independent

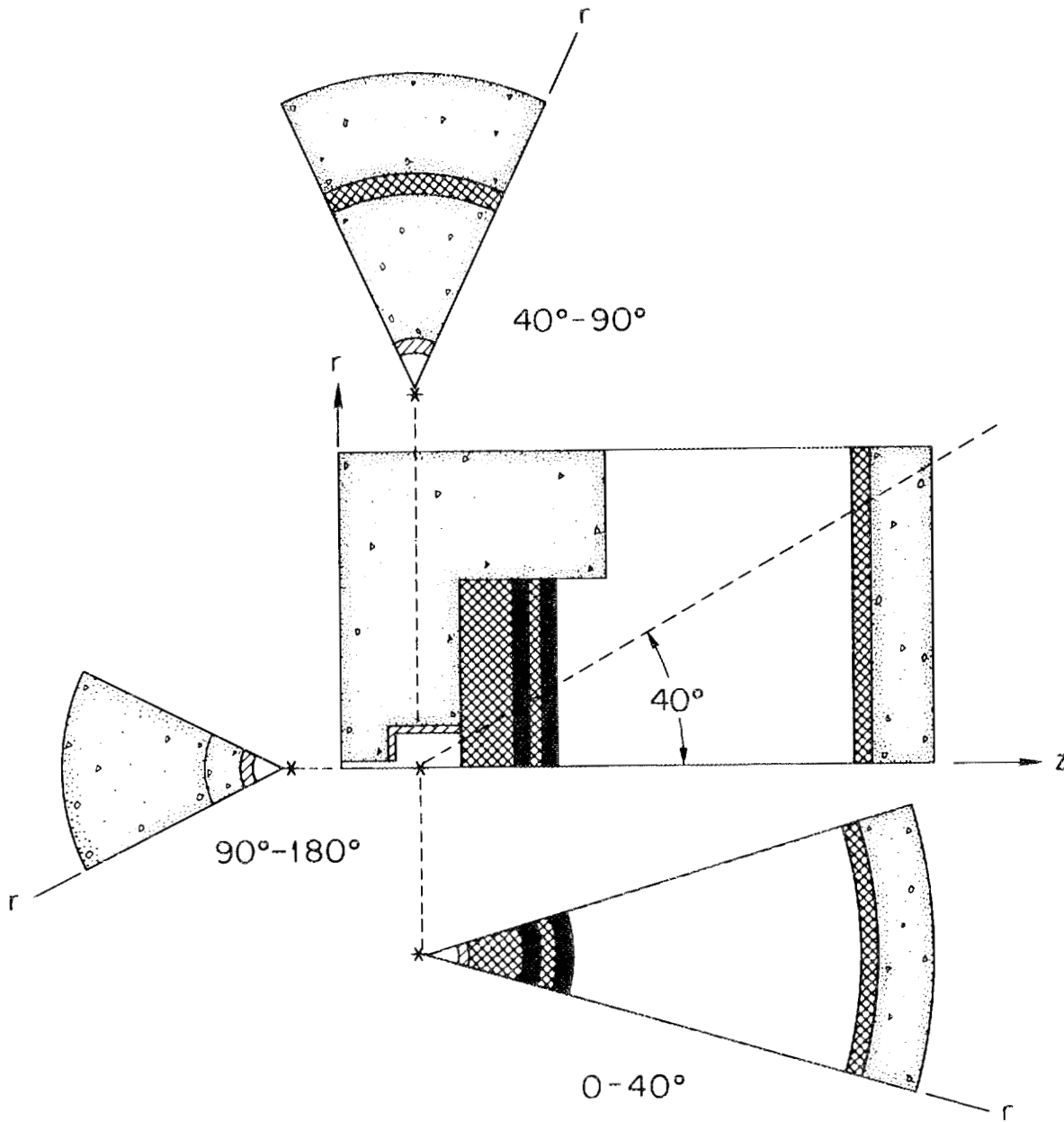


Fig. 18. Two-dimensional model of the experimental geometry with corresponding one-dimensional models for collapsing the cross section data.

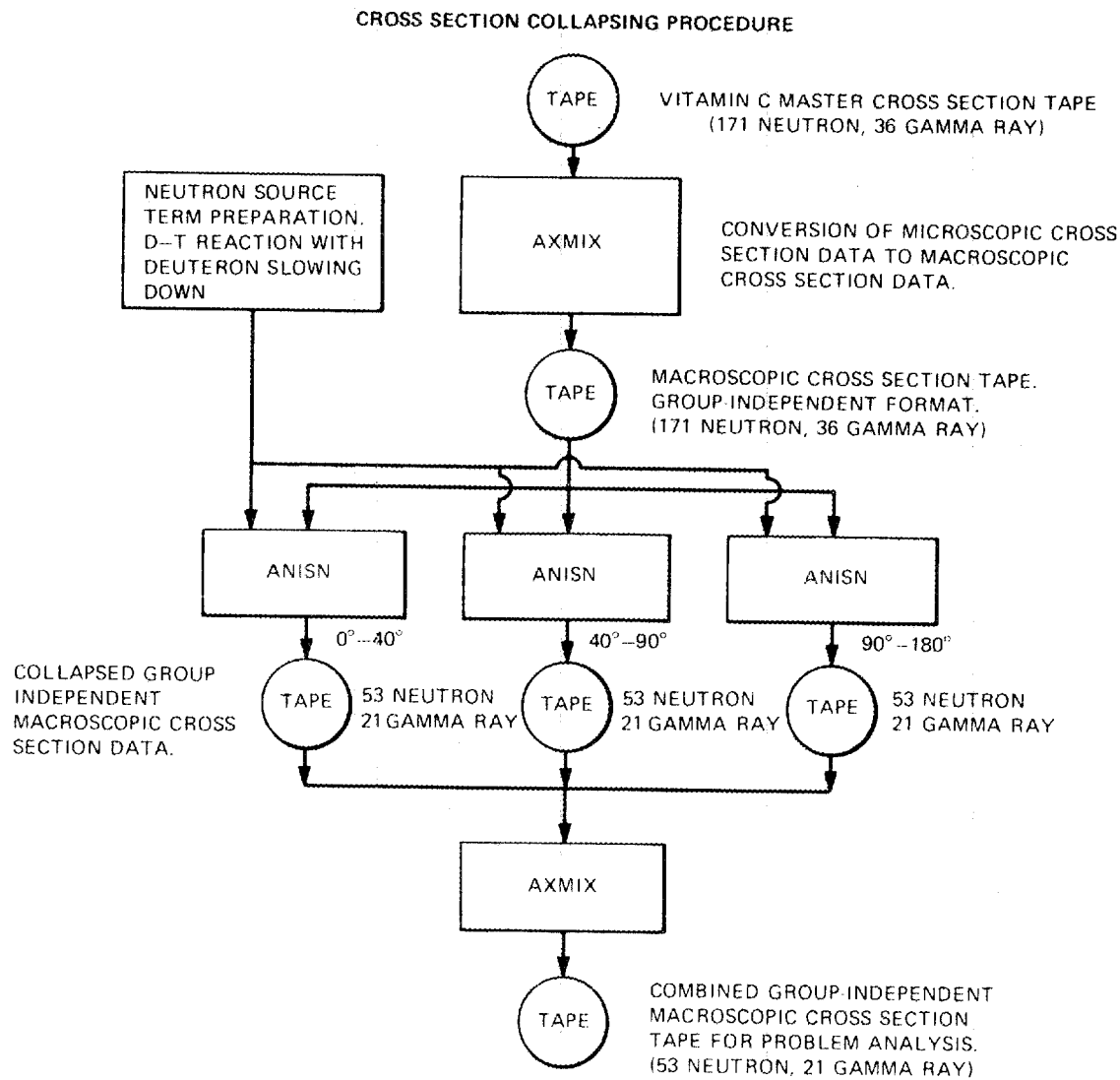


Fig. 19. Block diagram of the cross section collapsing procedure.

Table IV. Composition of Materials Used in the Calculation

Element	Composition (atom/cm ² •Barn)					Hevimet
	Concrete	Air	Iron Can	SS-304	BP*	
H	7.86x10 ⁻³				7.13x10 ⁻²	
B-10					4.87x10 ⁻⁴	
B-11					1.97x10 ⁻³	
C					3.41x10 ⁻²	
N		3.64x10 ⁻⁵				
O	4.39x10 ⁻²	9.74x10 ⁻⁶			3.64x10 ⁻³	
Na	1.05x10 ⁻³					
Mg	1.40x10 ⁻⁴					
Al	2.39x10 ⁻³					
Si	1.58x10 ⁻²					
K	6.90x10 ⁻⁴					
Ca	2.92x10 ⁻³					
Cr				1.77x10 ⁻²		
Mn				1.77x10 ⁻³		
Fe	3.10x10 ⁻⁴		8.48x10 ⁻²	6.02x10 ⁻²		
Ni				7.83x10 ⁻³		1.05x10 ⁻²
Cu						6.45x10 ⁻³
W-182						1.32x10 ⁻³
W-183						7.21x10 ⁻³
W-184						1.54x10 ⁻²
W-186						1.43x10 ⁻²

* BP = Borated Polyethylene

macroscopic cross section data sets were obtained and these were processed by AXMIX to form a combined macroscopic cross section tape for the analysis of the experiment.

Collapsing the data in this manner assures that the cross sections in each angular interval in the two-dimensional geometry of the experiment used in the analysis contain cross sections that have been weighted according to the source neutron energy distribution.

V. RADIATION TRANSPORT CALCULATIONS

The sequence of radiation transport calculations used to obtain the neutron and gamma ray energy spectra is shown in Fig. 20. The sequence is initiated by performing three separate calculations using the GRTUNCL code¹⁴ to obtain the uncollided neutron and first collision source distributions at all spatial mesh intervals in the calculational geometry. The purpose for performing these calculations separately is to account for the angle-energy dependence of the D-T neutron source. To insure that the contributions to the uncollided neutron flux and first collision sources were due to neutrons emitted into the angular intervals specified in Table II, black absorbers were interposed in the calculational geometry to confine the source neutrons to those angles. Also, the GRTUNCL code assumes isotropic neutron emission from a point source. To account for the anisotropy of the D-T neutrons the neutron angle-energy probabilities, $P(\Delta E, \Delta \theta)$, from Table II were weighted using a solid angle factor given by

$$P_w(\Delta E, \Delta \theta) = \frac{2P(\Delta E, \Delta \theta)}{\int_{\theta_1}^{\theta_2} \sin \theta' d\theta'} \quad (9)$$

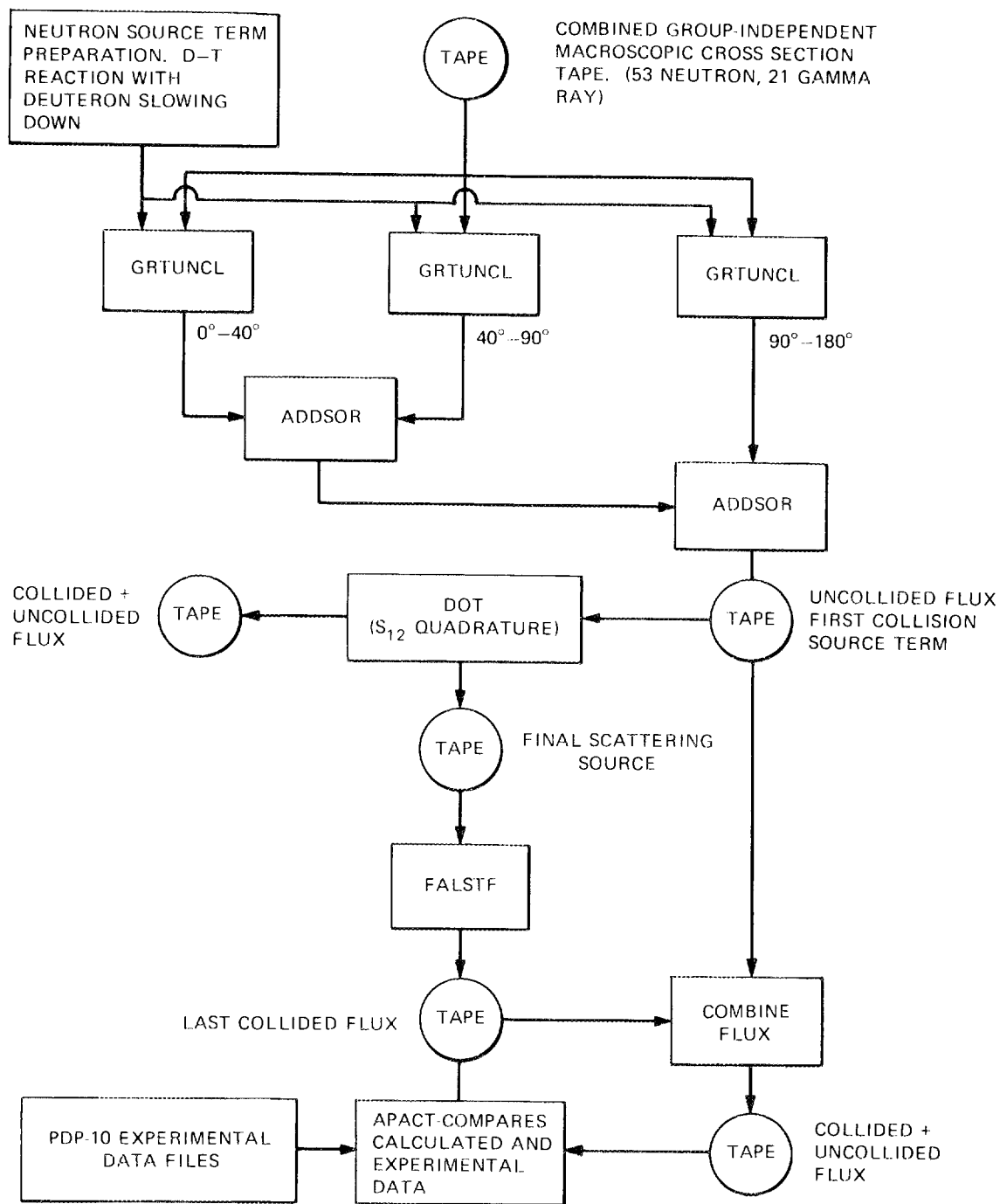


Fig. 20. Block diagram of the two-dimensional radiation transport code network.

where $P_W(\Delta E, \Delta \theta)$ is the solid angle weighted probability for neutrons in the energy interval ΔE emitted into the angular interval $\Delta \theta$ and θ is measured relative to the deuteron-target axis.

The first collision source data from each GRTUNCL calculation is combined to form a single source which is the input data to the two-dimensional discrete ordinates code DOT.⁶ This code calculates the collided flux distributions using the first collision data as a spatially distributed source. These calculations were completed using an S_{12} angular quadrature. A final scattering source tape is generated in DOT and is employed to carry out a last-flight transport calculation using the FALSTF code¹⁴ to obtain the neutron and gamma ray energy dependent flux at each detector location. The output from FALSTF is combined with the uncollided flux data from GRTUNCL to yield the total flux at each detector location. These total fluxes are processed to obtain the neutron and gamma ray energy spectra by smoothing the flux per unit energy in each multigroup energy interval with an energy-dependent Gaussian response function having a width determined by Eq. (2) for neutrons, and Eq. (3) for gamma rays. Performing the calculations in the sequence shown in Fig. 20 assures that ray effects from the D-T neutron source, as well as those from intense last collision sources from neutron reactions with experimental components are eliminated.

The necessity for incorporating such an extensive code network in the analysis of the attenuation experiments is best illustrated in Fig. 21. In this figure, measured and calculated neutron energy spectra are compared for the case of ~ 14 MeV neutron transport through a laminated shield composed of 30.48 cm of SS-304, 5.08 cm of borated polyethylene, and 5.08 cm

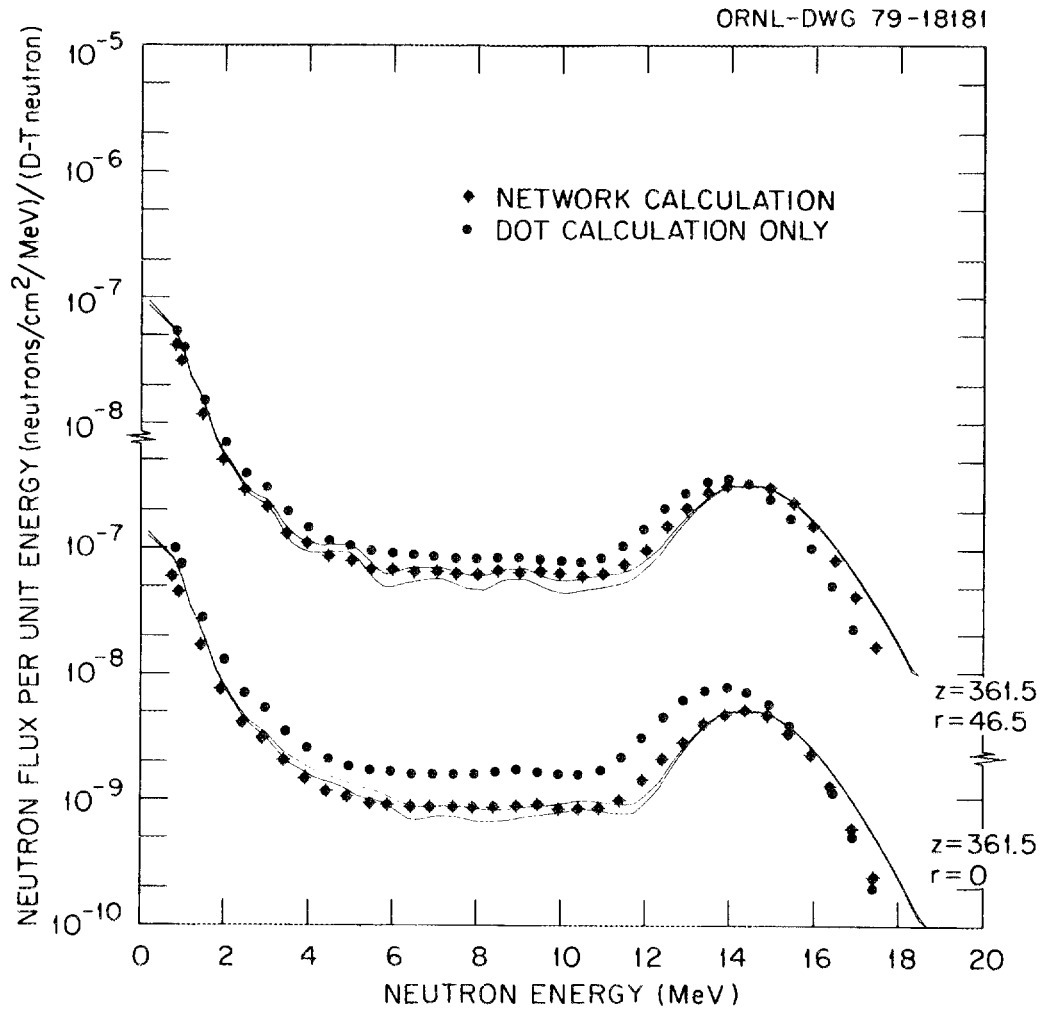


Fig. 21. Comparison of measured and calculated neutron spectra using network calculation and DOT calculation only.

of SS-304. The solid curves show the measured energy spectra at two detector locations on ($z = 0.0$) and off ($z = 46.5$) the axis of cylindrical symmetry. For each detector location, there are two solid lines which indicate the uncertainty in the energy spectra resulting from unfolding the pulse height data. Two sets of calculations are compared with the measured results: those obtained using the computer code network in Fig. 20 and those obtained using only the DOT code. The results obtained using only the DOT code overestimate the neutron spectra at all energies above 2 MeV for the detector both on and off the axis. On the other hand, the neutron spectra obtained using the network are in excellent agreement with the measured data.

It should be noted that the various codes comprising the network in Fig. 20 have in no way been modified or altered in any manner. The codes are "as delivered" from the Radiation Shielding Information Center. The codes have, however, been sequenced to take into account and treat many effects which improve the agreement among the measured and calculated results. GRTUNCL calculates the uncollided flux and first collision source distribution throughout the geometry mesh with the resulting elimination of ray effects that would occur with the point source — point detector treated in the model. The DOT code uses the GRTUNCL data as a source term and calculates the collided flux distributions. FALSTF treats the last flight of radiation from the geometry mesh to the detector.

The point to note is that the accurate analysis of radiation transport in fusion reactor blanket-shield assemblies and the determination of the effects of radiation on vital components of the reactor may require a more extensive analysis than might initially be considered, and that optimum use must be made of available computational tools.

REFERENCES

1. Y. Seki, R. T. Santoro, E. M. Oblow and J. L. Lucius, "Macroscopic Cross-Section Sensitivity Analysis for Fusion Reactor Shielding Experiments," Oak Ridge National Laboratory Report ORNL-5467 (1978).
2. Y. Seki, R. T. Santoro, E. M. Oblow and J. L. Lucius, "Comparison of One- and Two-Dimensional Sensitivity Calculations for a Fusion Reactor Shielding Experiment," Nucl. Sci. Eng. 73, 87 (1980).
3. R. T. Santoro, R. G. Alsmiller, Jr., J. M. Barnes and G. T. Chapman, "Calculation of Neutron and Gamma Ray Energy Spectra for Fusion Reactor Shield Design: Comparison with Experiment," Oak Ridge National Laboratory Report, ORNL/TM-7360 (1980); to be published in Nuclear Science and Engineering.
4. G. T. Chapman, G. L. Morgan and J. W. McConnell, "The ORNL Integral Experiments to Provide Data for Evaluating the MFE Shielding Concepts. Part I: Attenuation Measurements," Oak Ridge National Laboratory Report, ORNL/TM-7356 (in preparation).
5. W. R. Burrus and V. V. Verbinski, Nucl. Instr. Methods 67, 181 (1979).
6. W. A. Rhoades and F. R. Mynatt, "The DOT III Two-Dimensional Discrete Ordinates Transport Code," Oak Ridge National Laboratory Report, ORNL/TM-4280 (1979).
7. "BUGLE, Coupled 45-Neutron, 16-Gamma-Ray, P_3 Cross Sections for Studies by the ANS 6.1.2 Shielding Standards Working Group on Multigroup Cross Sections," DLC-47, Radiation Shielding Information Center, Oak Ridge National Laboratory (1977).

8. T. R. Fewell, "Absolute Determination of the 14-MeV Neutron Yields," SC-RR-67-346, Sandia Laboratory, Albuquerque, NM (1967).
9. "VITAMIN-C; 171-Neutron, 36-Gamma-Ray Group Cross Sections in AMPX and CCCC Interface Formats for Fusion and LMFBR Neutronics," DLC-41, Radiation Shielding Information Center, Oak Ridge National Laboratory (1978).
10. W. E. Ford, III, R. T. Santoro, R. W. Roussin and D. M. Plaster, "Modification Number One to the Coupled $100n-21\gamma$ Cross Section Library for EPR Calculations," Oak Ridge National Laboratory Report, ORNL-5249 (1976).
11. N. M. Greene et al., "AMPX: A Modular Code System for Generating Coupled Multigroup Neutron-Gamma-Ray Libraries from ENDF/B," Oak Ridge National Laboratory Report, ORNL/TM-3706 (1976).
12. W. W. Engle, Jr., "ANISN: A One-Dimensional Discrete Ordinates Transport Code with Anisotropic Scattering," Oak Ridge National Laboratory Report, K-1693 (1967).
13. "AXMIX, ANISN Cross Section Code," PSR-75, Radiation Shielding Information Center (1976).
14. R. A. Lillie, R. G. Alsmiller, Jr. and J. T. Mihalcz, Nucl. Technol. 43, 373 (1979).
15. "FALSTF, Informal Notes," CCC-351, Radiation Shielding Information Center (1979).

INTERNAL DISTRIBUTION

- | | | | |
|--------|---------------------------|--------|---|
| 1-2. | L. S. Abbott | 29. | RSIC |
| 3. | F. S. Alsmiller | 30-39. | R. T. Santoro |
| 4-8. | R. G. Alsmiller, Jr. | 40. | J. Sheffield |
| 9. | J. Barish | 41. | D. Steiner |
| 10-14. | J. M. Barnes | 42. | C. R. Weisbin |
| 15. | D. E. Bartine | 43. | G. E. Whitesides |
| 16. | L. A. Berry | 44. | A. Zucker |
| 17. | G. T. Chapman | 45. | P. Greebler (Consultant) |
| 18. | W. E. Ford, III | 46. | H. J. C. Kouts (Consultant) |
| 19. | T. A. Gabriel | 47. | W. B. Loewenstein (Consultant) |
| 20. | H. Goldstein (Consultant) | 48. | R. Wilson (Consultant) |
| 21. | R. A. Lillie | 49-50. | Central Research Library |
| 22. | F. C. Maienschein | 51. | ORNL Y-12 Technical Library -
Document Reference Section |
| 23-25. | E. M. Oblow | 52. | Laboratory Records |
| 26. | R. W. Peelle | 53. | ORNL Patent Office |
| 27. | R. W. Roussin | 54. | Laboratory Records - RC |
| 28. | M. W. Rosenthal | | |

EXTERNAL DISTRIBUTION

55. Office of Assistant Manager for Energy Research and Development, DOE-ORO, Oak Ridge, TN 37830
56. J. E. Baublitz, Office of Fusion Energy, Division of Development and Technology, MS G-234, U.S. Department of Energy, Washington, D.C. 20545
57. F. E. Coffman, Chief, Systems and Applications Studies Branch, Office of Fusion Energy, U.S. Department of Energy, Washington, D.C. 20545
58. B. Engholm, General Atomics Company, P.O. Box 81608, San Diego, CA 92138
59. C. R. Head, Office of Fusion Energy, MS G-234, U.S. Department of Energy, Washington, DC 20545
60. R. Ng, Office of Fusion Energy, U.S. Department of Energy, Washington, D.C. 20545
61. P. Sager, General Atomics Company, P.O. Box 81608, San Diego, CA 92138
62. Dr. Yasushi Seki, Japan Atomic Energy Research Institute, Tokai-mura, Ibaraki-ken, Japan
- 63-203. Given distribution as shown in TID-4500, Magnetic Fusion Energy (Distribution Category UC-20d: Fusion Systems)